



Cite this: DOI: 10.1039/d0gc02582h

Understanding the *in situ* state of lignocellulosic biomass during ionic liquids-based engineering of renewable materials and chemicals†

Kalavathy Rajan, ^a Thomas Elder, ^b Nourredine Abdoulmoumine, ^c
 Danielle Julie Carrier ^c and Nicole Labbé ^a

Ionic liquids (ILs) can be used to sustainably convert lignocellulosic feedstocks into renewable bio-based materials and chemicals. To improve the prospects of commercialization, it is essential to investigate the fate of lignocellulosic biomass during IL-based processing and develop tools for designing and optimizing this “green” technology. *In situ* characterization during pretreatment and dissolution processes have shown that ILs reduced the inherent recalcitrance of lignocellulosic biomass *via* swelling of cellulose bundles and formation of fissures in the secondary cell wall layers. It subsequently enhanced the penetration of ILs into the plant cell wall leading to depolymerization and solubilization of matrix polysaccharides, mainly hemicellulose *via* deacetylation. Lignin also underwent dehydration or reduction reactions, depending on the IL type, with different mechanisms leading to the cleavage of inter-unit linkages. Following this process, the accessibility to cellulose microfibrils increased and induced delamination. Complementary X-ray diffraction analyses have elucidated that ILs also reduced cellulose crystallinity and altered cellulose polymorphs. High throughput *in situ* analyses, namely bright-field optical microscopy, nuclear magnetic resonance and Fourier transform infrared spectroscopies, have aided in monitoring the degree of swelling and chemical structural changes in lignocellulosic biomass during IL-based processing. Development of novel *in situ* analytical tools like IL-based gel permeation chromatography and rheometry will further shed light on molecular level changes in lignocellulose. Thus, an overall understanding of physico-chemical changes underwent by lignocellulosic biomass will help develop tools for monitoring and improving IL-based engineering of renewable materials and chemicals.

Received 27th July 2020,
 Accepted 24th September 2020

DOI: 10.1039/d0gc02582h

rsc.li/greenchem

1. Introduction

Ionic liquids (ILs) are salts with very low melting points and therefore exist in a liquid state at room temperature.¹ They are composed of two parts, an organic cation and an inorganic or organic anion. Since an innumerable possible combination of cations and anions exist, ILs can be tailored for a broad range of applications in pharmaceuticals,² energy storage,³ heavy metal remediation,⁴ membrane filtration,⁵ lubrication,⁶ and for the synthesis of composite materials,⁷ to name a few. In the context of a biorefinery, ILs have demonstrated the unique capability to selectively dissolve lignocellulosic components or

bring about physico-chemical changes, which in turn can be exploited to produce biofuels and other value-added products.⁸ The beneficial properties of ILs, such as low vapor pressure, high thermal stability and tunable solvating capacity, are crucial to develop biochemical conversion platforms for utilizing renewable lignocellulosic feedstocks.^{9,10} However, the technology is in its nascent stage and the use of ILs for lignocellulosic biomass processing can be cost prohibitive.¹¹ Nevertheless, progress has been made in demonstrating the sustainability and potential economic feasibility of IL-based biomass processing technologies, and the prospects for commercialization are improving.^{12,13} For such developments to flourish, it is necessary to understand the critical role of ILs in dissolving and deconstructing lignocellulosic biomass.

Lignocellulosic feedstocks, such as agricultural residues, dedicated energy crops, and forest biomass,¹⁴ are sustainable and abundant sources of biopolymers, *i.e.*, cellulose, hemicellulose and lignin, that could be exploited as a replacement for petroleum-based chemicals and materials. Owing to the recalcitrant nature of lignocellulosic biomass, a multifaceted

^aCenter for Renewable Carbon, The University of Tennessee Institute of Agriculture, Knoxville, TN 37996, USA. E-mail: krajan@utk.edu, nlabbe@utk.edu

^bUSDA-Forest Service, Southern Research Station, Auburn, AL 36849, USA

^cDepartment of Biosystems Engineering & Soil Science, The University of Tennessee Institute of Agriculture, Knoxville, TN 37996, USA

†Electronic supplementary information (ESI) available. See DOI: 10.1039/d0gc02582h

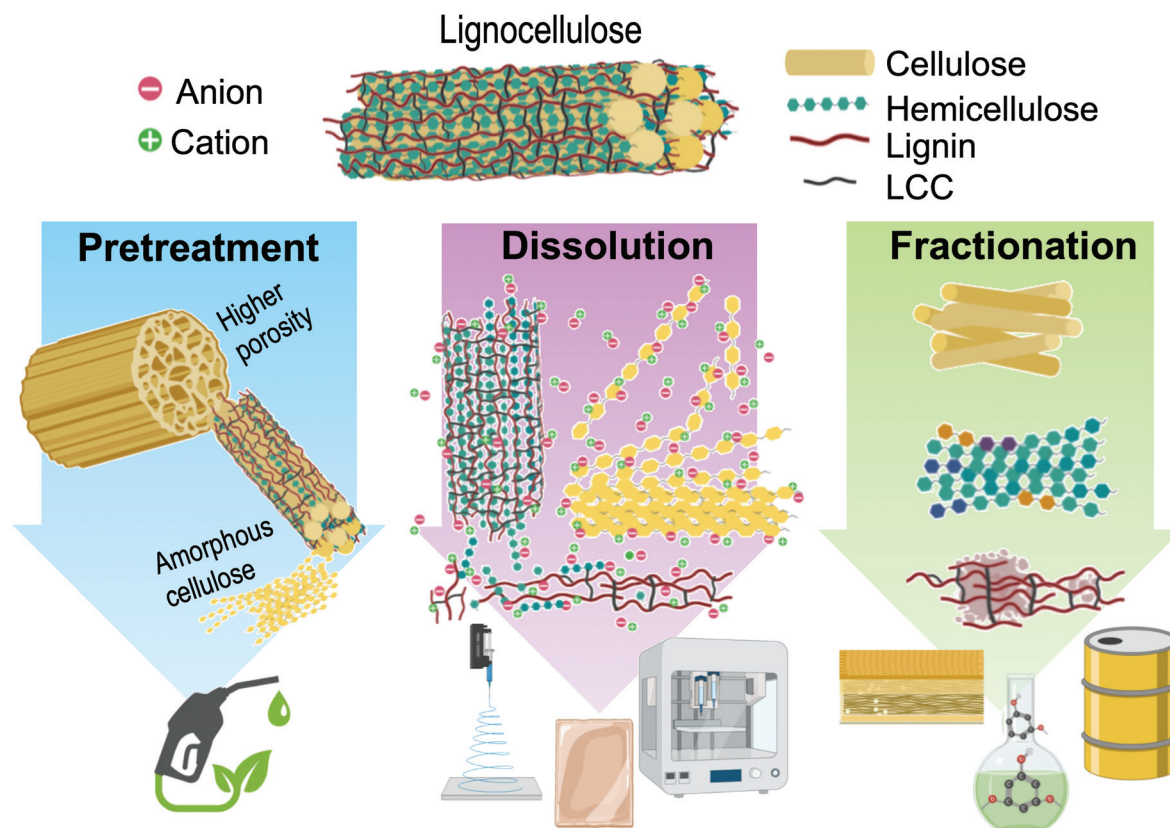


Fig. 1 Conversion of lignocellulosic biomass into value-added products using ionic liquids-based processing technologies. Pretreatment results in bulk morphological changes that favors biofuel production via enzymatic saccharification and fermentation. Dissolution results in delamination of cellulose, disruption of lignin-hemicellulose linkages that promote biomaterial processing like wet spinning, gelling and 3D printing. Fractionation provides opportunity to upgrade cellulose, hemicellulose and lignin biopolymers to platform chemicals, drop-in fuels and functional composites. (LCC – lignin carbohydrate complexes).



Kalavathy Rajan

Kalavathy Rajan is a Research Scientist with the Center for Renewable Carbon at the University of Tennessee-Knoxville, USA. She holds a Ph.D. degree in Food Science from the University of Arkansas-Fayetteville and did a Post-Doctoral Fellowship at the Dept. of Biosystems Engineering and Soil Science at UT-Knoxville. She was also an Indian Council of Agricultural Research International Fellow from

2012–2015 (New Delhi, India). Her research is concerned with the biochemical fractionation of lignocellulosic biomass, analytical and synthetic chemistry, as well as production of bio-derived polymers and materials.



Thomas Elder

Thomas Elder is a Research Scientist with the United States Department of Agriculture-US Forest Service. He holds a Ph.D. from Texas A&M University. He is an Emeritus Professor in the School of Forestry and Wildlife Sciences and Affiliate Professor in Biosystems Engineering at Auburn University. He is also an Adjunct Professor at the Center for Renewable Carbon at the University of Tennessee-Knoxville. He has been a visiting

scientist at the University of Wisconsin, the University of Copenhagen and the University of Natural Resources and Life Sciences, Vienna (BOKU). His research is concerned with the chemical characterization and utilization of wood. He is active in the application of computational chemistry to the reactions and structure of lignin.

physico-chemical and biochemical deconstruction strategy has to be employed to fractionate/isolate and utilize these biopolymers. IL-based processing is a facile approach for (i) pretreating lignocellulosic biomass for enhanced enzymatic saccharification, (ii) dissolving whole biomass or selective biomass constituents for material fabrication, and (iii) deconstructing and fractionating lignocellulosic biomass for subsequent upgrading (Fig. 1).

The effectiveness of biomass deconstruction is determined by the composition and properties of ILs. For example, ILs with stronger hydrogen-bonding anions can selectively fractionate cellulose,^{15,16} whereas those with planar cations were shown to be more effective in fractionating lignin.¹⁷ Similarly, ILs with high polarity, where either the cation or anion is coupled with a strong hydrogen-bonding counterpart, have displayed significantly improved dissolution capacity of whole lignocellulosic biomass.^{18,19} Biomass deconstruction depends greatly on the ability of the IL to form intermolecular interactions with lignocellulosic components where the strength of interaction can be tuned by modifying the chemical composition.²⁰ There are empirical scales that predict hydrogen bonding and solvating capacity of ILs based on their chemical formulae,^{21,22} however, very few approaches have directly measured the *in situ* state of lignocellulose during treatment with ILs. Previous publications have critically investigated the interactions between IL-cations, anions and lignocellulosic components in order to compose more efficient ILs, and provided strategies for process design.^{10,23} However, challenges still remain in characterizing the *in situ* state of lignocellulose during the process development stage, without which there will be hurdles for new technology development, maturation, and deployment.

Therefore, in this review, we will investigate the *in situ* state of lignocellulosic biomass during IL-based processing in order

to bridge the gap between available knowledge for IL design and feasible technologies for bio-materials/chemicals production. *In situ* characterization studies employing small-angle neutron scattering, optical microscopy, infrared and nuclear magnetic resonance spectroscopy have identified the bulk and supramolecular structural changes during IL-treatment of lignocellulosic biomass. Complementary characterization using scanning electron microscopy, chemical composition analysis, crystallinity measurement and molecular weight determination have provided a wholistic understanding of the morphological and physico-chemical changes effected by ILs. Development of high throughput screening tools, which employ these *in situ* characterization techniques, will be the stepping stones for attaining higher process efficiency and for designing new applications. Hence, this review will provide comprehensive insights about the various physico-chemical transformations of lignocellulosic biomass, as well as furnish the tools for designing and optimizing IL-based “green” material processing technology.

2. Current status of IL-based lignocellulose processing

ILs have been used to process different types of lignocellulosic biomass, such as agricultural residues, dedicated energy crops and forest biomass (Table 1). Lignocellulosic feedstocks are composed of 24–53% of cellulose, 15–39% hemicellulose, 7–30% lignin, 1–12% organic extractives and 1–6% ash.²⁴ The biopolymers constituting these feedstocks *i.e.*, cellulose, lignin and hemicellulose, are rich and abundant sources of biologically and industrially relevant chemicals, namely glucose, xylose, galactose, mannose, arabinose, monophenols, polyphene-



Nourredine Abdoulmoumine

into energy, refinery-ready intermediates, chemical building blocks or advanced fuels through the use of thermochemical conversion technologies like gasification and pyrolysis.

Nourredine Abdoulmoumine is an Assistant Professor at the Department of Biosystems Engineering and Soil Science at the University of Tennessee-Knoxville, USA. He holds a Ph.D. in Biosystems Engineering from Auburn University, Alabama, and is the founder of Biomass conversion And Modeling (BEAM) laboratory at UT-Knoxville. His research interests are centered on the conversion of lignocellulosic biomass



Danielle Julie Carrier

research interests include promoting the use of renewable energy production, specifically biofuels and biochemicals from lignocellulosic biomass, and she has twice won recognition as an outstanding researcher. She is also known for her ability to provide outstanding service to students. Dr Carrier has won four student service and teaching awards since 2003.

Danielle Julie Carrier is the Professor and Head of Department of Biosystems Engineering and Soil Science at the University of Tennessee-Knoxville, USA. She holds a Ph.D. in Chemical Engineering from McGill University, Quebec, Canada, and served as a professor in the College of Engineering, Department of Biological and Agricultural Engineering at the University of Arkansas-Fayetteville. Her

nols, and hydrocarbons. In addition to bioenergy applications, these bio-derived components are useful for the synthesis of “green platform chemicals” like ethanol, butanol, 5-hydroxymethylfurfural, furfural, propylene glycol, 3-hydroxy-propionic acid, butyric, fumaric, succinic, itaconic, malic acid, xylitol, and 2,5-furandicarboxylic acid,²⁵ and “green materials” like carbon fiber,²⁶ thermosets,²⁷ nanomaterials,²⁸ and functional packaging.²⁹

At first, ILs were utilized to dissolve purified cellulose for the purpose of developing sustainable and eco-friendly material fabrication technologies.³⁰ Afterwards, new ILs were synthesized to directly dissolve lignin,¹⁷ as well as whole lignocellulosic biomass.³¹ As a result, utilization of otherwise recalcitrant plant biomass for thermal and bio-chemical conversion platforms became possible.³² Common types of cations and anions used in the design of ILs for lignocellulosic biomass processing are provided in Fig. 2; a more exhaustive list has been published elsewhere.^{10,33} As shown in Fig. 2, modern ILs are made with organic cations like quaternary ammonium with aromatic and aliphatic functionality, alkylated phosphonium and even bio-based choline ions. Generally, IL-anions are organic or inorganic in nature, including novel amino acid-based molecules, except for halides that are polyatomic. The mechanisms involved in the dissolution of lignocellulosic components by ILs are critical for developing biomass conversion technologies. The following sections will summarize different strategies involved in the deconstruction of lignocellulosic biomass using ILs.

2.1. Lignocellulose pretreatment

Depending on the end-product, different strategies are applied to process lignocellulosic feedstocks. The most common strategy *i.e.*, pretreatment or pre-conditioning, is applied to



Nicole Labbé

Nicole Labbé is a Professor of Biomass Chemistry in the Center for Renewable Carbon, with an academic appointment in the Department of Forestry, Wildlife & Fisheries at the University of Tennessee-Knoxville, USA. She received her Ph.D. in Wood Sciences from the University of Bordeaux, France. Her research focuses on understanding properties of lignocellulosic biomass—appearance, variability, and potential for conversion to

various products such as fuels, chemicals, and value-added materials. Specifically, she studies novel biological and chemical routes to directly convert and/or fractionate biomass into bio-based products. Ultimately, Dr Labbé's research aim is to provide detailed understanding of plant cell walls; their roles in plant function; and anatomical, physical, and chemical factors that control biomass recalcitrance during conversion.

produce second-generation biofuels. As the name implies, pretreatment is the initial stage of biomass processing in a biorefinery which primarily facilitates the near-complete hydrolysis of cellulose during the subsequent stages. Pretreatment of lignocellulosic biomass using ILs generally results in physical and chemical changes to the plant cell wall, including an increase in pore size, decrease in cellulose crystallinity, increase in accessible surface area to cellulolytic enzymes and partial removal of hemicellulose or lignin.^{10,11} Different types of ILs, composed of methylimidazolium, pyrrolidinium, morpholinium and choline cations in combination with carboxylate, triflate, methanesulfonate, amino acid and chloride anions, have been utilized for biomass pretreatment purposes (Table 1). As a result of pretreatment with ILs, the production efficiency of glucose during enzymatic saccharification was shown to increase by up to 96%,³⁴ and ethanol yield during fermentation improved by up to 64%.³⁵ In addition to the benefits of increased process efficiency, ILs used for pretreatment can be recycled which enhances the sustainability and eco-friendly aspects of this technology.

2.2. Lignocellulose dissolution

Dissolution is another technique commonly used to process lignocellulosic biomass. As given in Table 1, choline,⁷¹ quaternary ammonium,⁷² and methylimidazolium cations in combination with carboxylate, chloride,^{57,70} amino acid,⁷² and phosphonium anions have been reportedly used to completely dissolve various herbaceous and woody feedstocks. Unlike pretreatment where the lignocellulosic components are only partially removed to reduce recalcitrance, the dissolution process is aimed at bringing the entire plant biomass to a solution state. The advantage of whole biomass dissolution is that it facilitates subsequent catalytic depolymerization for the production of platform chemicals like guaiacol.^{48,49} In addition, the regenerated biomass could be utilized for the fabrication of novel composites,^{55,56} and films,⁵⁷ that exhibit improved thermotolerance and mechanical performance. The dissolution technique also provides a significant advantage to conventional blending and wet spinning technology, because ILs can act as plasticizers and assist in the extrusion of otherwise intractable lignocellulosic biomass.^{63,73} ILs can also be used to induce thermo-reversible cross-links between the lignocellulosic components upon regeneration, which provides unique opportunities to tune the structural and chemical properties of resulting matrices.⁷⁰ Specifically, ILs containing phosphonium⁶⁷ and trifluoromethylsulfonyl⁶⁶ anions have been used to chemically modify the hydroxyl groups of lignocellulose during dissolution which in turn altered the polymerization behavior of the regenerated material. Overall, the facility to dissolve whole lignocellulosic biomass proffers abundant opportunities for the future development of IL-based material processing technologies.

2.3. Lignocellulose fractionation

Apart from pretreatment and dissolution, ILs can also be used to fractionate/isolate the components of lignocellulosic

Table 1 Techniques for processing lignocellulosic biomass using ionic liquids

Processing technique	Biomass	Ionic liquid	Bio-based product	Ref.
Biofuel, value-added intermediates				
Pretreatment, enzymatic saccharification, fermentation	Rice straw	1- <i>H</i> -3-Methylmorpholinium chloride	Ethanol	35
	Sunflower stalk	1-Butyl-3-methylimidazolium chloride	Ethanol	36
	Sugarcane bagasse, Rice straw	Cholinium lysinate, cholinium arginate	Fermentable sugars	37 and 38
Fractionation	Oil palm fruits	1-Butyl-3-methylimidazolium chloride	Lignin	39
	Barley straw	1-Ethyl-3-methylimidazolium acetate	Holocellulose, lignin	40
	Bagasse, Southern yellow pine	Choline acetate	Cellulose, hemicellulose, lignin	41
	Japanese cedar	<i>N</i> -Methyl- <i>N</i> -(2-methoxyethyl)pyrrolidin-1-ium 2,6-diaminohexanoate	Lignin, holocellulose	42
Catalysis and production of platform chemicals				
Catalytic dehydration	Corn stover	1-Ethyl-3-imidazolium chloride	5-HMF	43
	Sugarcane bagasse	1-Methyl-3 (3-sulfopropyl)-imidazolium hydrogen sulfate	Furfural	44
Catalytic redox reactions	Technical lignin	1-Butyl-3-methylimidazolium chloride	Acetic acid	45
	Acid-catalyzed hydrolysis	Rubber wood, Oil palm frond, Bamboo, Rice husk	1,4-Bis(3-methylimidazolium-1-yl) butane tetrahydrogen sulfate	Levulinic acid
Catalytic hydrogenolysis	Kraft lignin	Choline methanesulfonate	Phenol, catechol	47
	Dissolution, regeneration & depolymerization	Eucalyptus, Pine, Switchgrass, Oak wood	1-Ethyl-3-methylimidazolium acetate, 3-methylimidazolium chloride, 1-ethyl-3-methylimidazolium chloride	Guaiacol, vanillin, syringol
Oxidative depolymerization	Beech lignin	1-Ethyl-3-methylimidazolium trifluoromethanesulfonate	Vanillin	50
	Kraft lignin	1-Ethyl-3-methylimidazolium acetate	Guaiacol, syringol, acetovanillone	51
	Japanese cedar	Tetrabutylammonium hydroxide 30-hydrate	Vanillin, vanillic acid	52
Fractionation, depolymerization	Eucalyptus, Southern pine, Norway spruce pulp	1-Allyl-3-methylimidazolium chloride	Furfural, HMF, catechol, methylcatechol, methylguaiacol	53
Pretreatment, enzyme-mediated transglycosylation	Cellulose	Tetrabutylphosphonium glycine	Methyl β -D-glucoside	54
Fabrication of renewable materials & surfaces				
Dissolution, regeneration, compounding & molding	Cotton, Aspen wood	1-Ethyl-3-methylimidazolium acetate	Composite boards	55
	Oil palm fronds	1-Butyl-3-methylimidazolium chloride, 1-ethyl-3-methylimidazolium diethyl phosphate	Composite boards	56
	Chinese fir	1-Allyl-3-methylimidazolium chloride	Composite films	57
	Bagasse, Hybrid poplar	1-Butyl-3-methylimidazolium chloride, 1-ethyl-3-methylimidazolium acetate	Lignocellulosic films	58 and 59
Dissolution, ink-jet printing & coagulation	Cellulose	1-Ethyl-3-methylimidazolium acetate, 1-butyl-3-methylimidazolium acetate	High-resolution 3D structures	60 and 61
Dissolution, wet spinning, electrospinning & coagulation	Southern yellow pine, Bagasse, Hybrid poplar	1-Ethyl-3-methylimidazolium acetate	Lignocellulosic macro-fibers	62 and 63
	Eucalyptus pulp, Kraft lignin	1,5-Diazabicyclo[4.3.0]non-5-enium acetate	Composite fibers	64
Chemical modification & molding	Hemp	1-Ethyl-3-methylimidazolium acetate	Lignocellulosic nanofibers	65
	Pine wood	Didecyl-dimethylammonium-bis (trifluoromethylsulfonyl) imide	Bio-based thermoplastic	66
	Bagasse, Japanese cedar, Eucalyptus	1-Ethyl-3-methylimidazolium methylphosphonate	Flame-retardant thermoplastic	67
Dissolution, organocatalytic oxidative/trans-esterification	Cellulose, Sugarcane bagasse	1-Ethyl-3-methylimidazolium acetate	Cellulose ester	68 and 69
Dissolution, freeze-thaw cycling	Norway spruce	1-Butyl-3-methylimidazolium chloride	Bio-based hydrogels	70

biomass. Polar and non-polar, IL-based solvent systems have been designed to facilitate liquid-liquid extraction of cellulose, hemicellulose and/or lignin based on their solubility parameters.^{8,40,74} ILs composed of imidazolium, organoammonium cations and hydrogen sulfate, chloride anions have been previously reported for this purpose (Table 1). The fractionated lignocellulosic components may be utilized as they are, or sub-

jected to additional IL-based processing to produce second-generation biofuels,^{11,74} or platform chemicals like furfural, phenol, catechol, methylcatechol, methylguaiacol and 5-hydroxymethylfurfural.^{44,47,53} Recently, catalytic depolymerization and upgrading techniques involving hydrogenolysis,⁴⁷ acid hydrolysis,⁴⁴ oxidation,⁵¹ and dehydration^{43,44,75} have been employed to valorize IL-fractionated lignin and structural

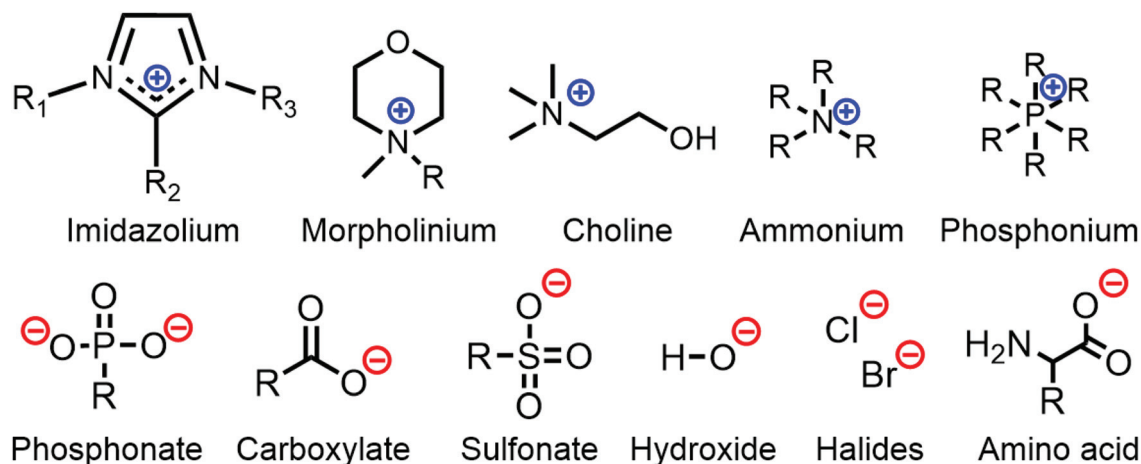


Fig. 2 Common cations and anions that constitute ILs used for pretreatment, dissolution and fractionation of lignocellulosic biomass.

carbohydrates. Thus, IL-based fractionation provides the opportunity to reduce waste and valorize all lignocellulosic components such that it enhances the techno-economic feasibility of biorefinery operations.

3. Design and evaluation of IL-based solvent systems

It is important to carefully select the cationic and anionic components of ILs since chemical composition will determine the physico-chemical properties and application of ILs in lignocellulosic biomass processing. There are semi-empirical prediction models as well as empirical scales available for categorizing the IL-cations and anions based on chemical behavior. Parameters affecting the selection of IL components are hydrogen bond basicity, hydrogen bond acidity, bond polarizability and overall solvating capacity.¹⁵ Hydrogen bond basicity measures the ability of an anion to accept protons, hydrogen bond acidity measures the ability of a cation to donate protons and bond polarizability measures the separation of electric charge along a bond. These parameters are useful for understanding molecular level interactions between solute-solvent and solvent-solvent systems, as well as for drawing correlations between the molecular structure and solvating capability of ILs.

3.1. Pre-screening of ILs using empirical polarity scales

Traditional empirical scales, like Reichardt's $E_T(30)$, utilize a solvatochromic pyridinium *N*-phenolate betaine dye to spectroscopically measure the polarity of ionic liquids.⁷⁶ $E_T(30)$ determines the molar transition energy of a standard betaine dye in the presence of a solvent system, where higher $E_T(30)$ values corresponds to a highly polar nature.⁷⁶ Reichardt has listed the polarities of about 80 different ILs composed of ammonium, tetraalkylphosphonium, alkylimidazolium, alkylpyridinium cations and carboxylate, methanesulfonate, halide anions.⁷⁶ ILs with very low hydrogen bond acidity (α) ranked

on the apolar side of the $E_T(30)$ scale, whereas those with higher α values leaned towards the polar end.

The importance of hydrogen bonding capacity of the ILs is further elucidated by the Kamlet-Taft's polarity scale,^{21,22} where a set of solvatochromic probes are used to measure multiple parameters, including solvent dipolarity/polarizability, hydrogen bond acidity and hydrogen bond basicity. The dipolarity/polarizability parameter, π^* , is used to measure the ability of ILs to stabilize a charge or become polarized.⁷⁷ It is determined based on the change in maximum absorption energy of a solvatochromic dye that has been induced by the local electric field created by a solvent.⁷⁸ The π^* value has been recorded for over 150 ILs and the main property found to affect the polarity scale was the alkyl chain length of the cation; longer alkyl chain length led to decrease in IL polarity.^{78,79} The hydrogen bond acidity (α) of ILs was also found to be affected by the alkyl chain length, since the α values decreased significantly with the alkylation of acidic positions in cations.⁷⁹ On the other hand, hydrogen bond basicity (β) of ILs depended on the strength of anions; for example, halide and azide anions exhibited the highest β values by virtue of their strong electronegativity.⁷⁹

Both α and β parameters are critical for designing novel solvent systems, because they determine the interactions between ILs and solutes like lignocellulosic biomass. The common modes of interactions between ILs and lignocellulosic biomass are depicted in Fig. 3a-c. It has been reported that ILs with acidic cations and high α values can form hydrogen bonds with ether and hydroxyl groups of lignin, thereby resulting in effective delignification.¹³ Similarly, ILs with highly electronegative anions and comparatively higher β parameter can form electron donor-acceptor complexes with the hydroxyl groups of cellulose, thereby weakening the intermolecular hydrogen bonds and resulting in defibrillation.^{80,81} Subsequent studies have shown that formation of electron donor-acceptor complexes (Fig. 3c) between ILs and lignocellulosic biomass is essential for fractionation or dissolution processes.⁶³

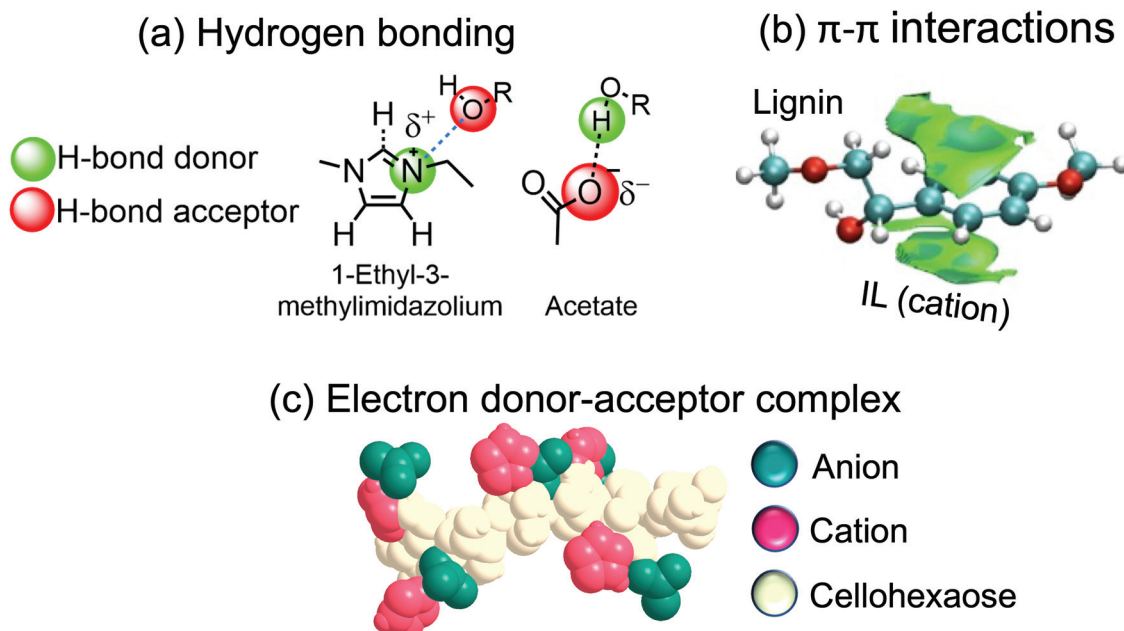


Fig. 3 Modes of interaction between ionic liquids and lignocellulose. (a) Hydrogen bonding between the hydroxyl groups of cellulose/lignin and 1-ethyl-3-methylimidazolium acetate; (b) π - π stacking between the aromatic rings of lignin and IL-cation ring (adapted from ref. 86 with permission from Elsevier); and (c) formation of electron donor/acceptor complexes between hydroxyl groups of cellohexaose (model for cellulose), acetate ion and 3-methylimidazolium ion.

Semi-empirical polarity scales can also be developed using computational methods to predict the hydrogen bond basicity and other solvent-interaction parameters of ILs.^{13,81} For example, the molecular dynamics simulation-based COSMO-RS method (CONductor-like Screening Model for Real Solvents) was adapted to predict the β values of ILs based on the unimolecular quantum calculations of hydrogen-bonding energies for specific cation-anion pairing.^{82,83} Cross validation using experimentally determined values showed that COSMO-RS can successfully predict the β parameter for IL co-solvent systems.^{82,83} Other means for utilizing molecular dynamic simulations are to predict the changes in conformational and interaction energies between IL-cation, anion and lignocellulosic polymers.^{84,85} Such simulations can shed light on the formation of electron donor-acceptor complexes between ILs and lignocellulose, as well as draw correlations between IL chemical composition and dissolving capability.⁸¹ Henceforth, development of predictive tools like COSMO-RS is crucial for screening ILs based on the application and for selecting anions and cations that favor IL-biomass interactions.

3.2. Solubility parameters to design high performance IL-based systems

Understanding the interactions between lignocellulosic components, ILs and other molecular solvents like water is essential for the design of an efficient fractionation or dissolution process. Addition of co-solvents to ILs can improve the formation of electron donor-acceptor complexes by changing interaction energies. On the other hand, anti-solvents will

compete for interactions with ILs thereby interfering with their capability to form electron donor-acceptor complexes and result in the precipitation of dissolved polymers (Fig. 4). Generally, hydrogen bond donating species (high α) are chosen as anti-solvents, whereas hydrogen bond accepting species (high β) are chosen as co-solvents for IL-lignocellulose systems.⁸⁷ Different types of molecular liquids like water,⁸⁸

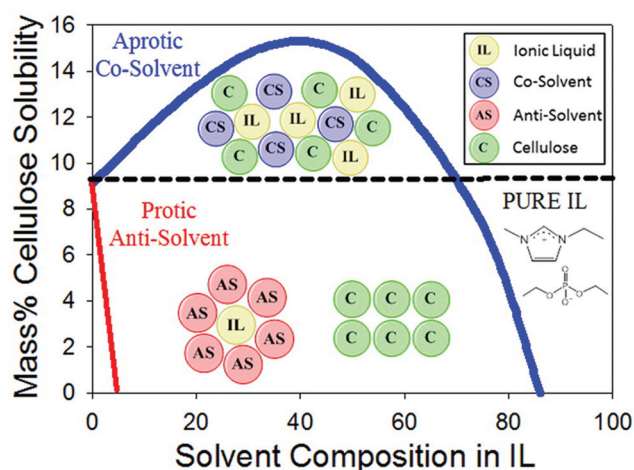


Fig. 4 Relationship between ionic and molecular liquids in selectively dissolving and regenerating the constituents of lignocellulosic biomass. The relative solubility of cellulose in ILs like 1-butyl-3-methylimidazolium chloride was evaluated in the presence of co-solvents like DMSO, DMF, and anti-solvents like water and ethanol. Reproduced with permission from ref. 87; copyright (2016) American Chemical Society.

DMSO,^{89,90} dimethylformamide,⁹¹ acetonitrile,⁹¹ 2-phenoxyethanol,⁹² γ -valerolactone⁹³ and acetic acid,⁹⁴ have been evaluated for co-dissolution of cellulose and lignin. These co-solvents can be pre-screened using computational tools, where empirical parameters based on Hansen or Hildebrand solubility theories could supply necessary background information.^{88,92} The Hildebrand solubility parameter (δ_H) measures the amount of energy required to disrupt the intermolecular interactions and arrangements between solvents and solutes, and it can be measured using heat of vaporization, intrinsic viscosity, osmotic pressure or inverse gas chromatography.^{88,95} The Hansen solubility theory provides a comprehensive estimate of the radius of interaction between the solute and solvent molecules based on dispersion, dipole–dipole and hydrogen bonding forces. The smaller the size of Hansen solubility sphere, when compared to that of lignocellulosic components, the higher will be the solvating capacity of ILs.³³ Studies have shown that evaluation of differential solvating capacity of ionic and molecular liquid mixtures is essential for the improvement of fractionation yields; up to 90% of hemicellulose and 60% of lignin have been reportedly recovered from woody and herbaceous feedstocks based on predictions made by δ solubility parameters.^{88,92} An extensive list of δ solubility parameters for 24 different ILs, along with 45 different co-molecular solvents, has been published elsewhere.^{95–97}

In summary, the different empirical parameters namely $E_T(30)$, π^* , α , β , and δ_H are useful for estimating the interactions between lignocellulose and ILs. Some computational methods may even provide insights into the mechanism of dissolution by ILs and propose compositional changes that may improve the processing yields.⁸² However, these empirical or computational methods are not sufficient to support the development of IL-based biomass processing technologies. For that, real-time or post-regeneration measurement of physico-chemical properties of lignocellulose is required. The ensuing section will elaborate on *in situ* investigations of structural and chemical changes in lignocellulosic biomass, such that it will advance the process development and optimization of IL-based conversion technology.

4. Contemporary evaluation of lignocellulose during IL-processing

4.1. Mechanism of swelling and unraveling of cell wall layers

In situ characterization of lignocellulosic biomass using optical microscopy has been useful for screening and high throughput evaluation of ILs.^{8,98,99} Studies using bright-field optical microscopy have shown that, at higher temperatures of 120 to 160 °C, lignocellulosic biomass rapidly dissolve in ILs in as little as 80 minutes.^{31,57,100,101} As shown in Fig. 5a and b, the fiber bundles of sawdust disappeared completely within 4 h, thereby signifying the end of dissolution process. These studies were conducted at a length scale of 10 μm to 2 mm, which captured only the bulk deconstruction of the plant cell network. For a detailed analysis, introduction of cross-polarizing filters has been shown to capture the changes in cellulose crystallite structure at a length scale of 20 to 200 μm .^{102–104} The chiral nematic property of cellulose crystallites is known to produce birefringent patterns when observed between crossed polarizers (Fig. 5c and d). During exposure to ionic liquids the birefringent pattern disappears in 0.3 to 72 h, even at a low temperature of 50 °C, because of the disassembly of the crystalline arrangement of cellulose.^{102–104} It was proposed that, breakage of inter-molecular and inter-chain linkages, as a result of hydrogen bonding interactions with ILs, was the prime reason for cellulose crystallinity decrease.^{103,104} Loss of cellulose crystallinity is also the first step towards reducing the recalcitrance of lignocellulosic biomass, as it precedes the complete solubilization of the plant cell wall network.¹⁰²

Changes occurring in the secondary and middle lamellar layers of plant cell wall, during IL-based processing, can be recorded using confocal microscopy, which provides a comparatively enhanced spatial resolution at a length scale of 0.5 to 3 μm .^{102,105,106} The confocal images can be mapped according to chemical composition, using either autofluorescence of lignin or differential vibrations of lignocellulosic components in the Raman spectrum.^{105,107} Raman imaging is conducted in the range of 2830–2920 cm^{-1} for polysaccharides and

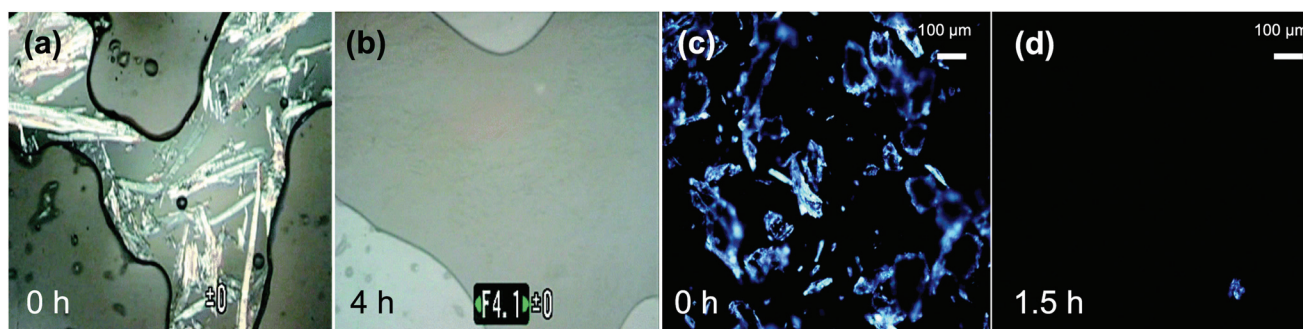


Fig. 5 (a and b) Optical microscopy images depicting the time dependent *in situ* dissolution of Norway spruce sawdust in 1-allyl-3-methylimidazolium chloride at 120 °C. Disappearance of fiber bundles is used to determine the end-point of biomass dissolution. Adapted with permission from ref. 31; copyright (2007) American Chemical Society. (c and d) Polarized light microscopy images of microcrystalline cellulose during dissolution in 1-ethyl-3-methylimidazolium acetate at 50 °C. Changes in cellulose crystallinity are captured using this technique, as a function of time. Adapted from ref. 104 with permission from the Royal Society of Chemistry.

1550–1650 cm^{-1} for lignin at an emission wavelength of 532 or 785 nm.^{102,105–107} Confocal Raman microscopy-based tissue mapping has consistently shown that the polysaccharides in secondary cell wall layers swell in the presence of ILs, followed by distortion and shrinkage of middle lamellar layer, which facilitates the dissolution of lignin naturally aggregated in this layer (Fig. 6A). The degree of swelling of secondary cell wall, changes in the total dimension of individual cells and changes in the intensity of Raman vibrational spectra have been used to qualitatively estimate the impact of ILs on lignocellulosic biomass.^{102,105–107} Evaluations based on Raman imaging showed that IL anions with higher hydrogen bond basicity were capable of significantly higher interactions with the hydroxyl groups of cellulose and hemicellulose resulting in the observed swelling of secondary plant cell wall layers.¹⁰⁸ It was also clear from these studies that, access and diffusion of ILs through lignocellulosic polymers played a critical role during cell wall dissolution. As a side note, conventional and Raman optical microscopies are limited by the diffraction of light, and breaking this diffraction limit by focusing on single molecular emission or scattering can help to achieve ultra-high resolutions. State-of-the-art techniques like super localization microscopy can provide spectrally and temporally-resolved nano-scale images, which will be ideal for investigating cellulose crystallite level changes. A full review of optical microscopy techniques for the nano-scale characterization of solution state polymers has been published elsewhere.¹⁰⁹

In addition to *in situ* microscopic examinations, gross morphological changes occurring in regenerated lignocellulosic substrates, at a scale of 5 to 100 μm , have been utilized to screen the ILs.^{102,108,110} Scanning electron microscopy (SEM) studies have shown that treatment with ILs at higher temperatures of 120–155 $^{\circ}\text{C}$ resulted in increased porosity, disruption of cell center and middle lamellar regions, unravelling of secondary cell wall layers and consequent delamination of wood fibers (Fig. 6B).^{102,108,111} Appearance of pores after IL-pretreatment was attributed to delignification, whereas disruption of cell center and middle lamellae was attributed to the preliminary swelling of secondary cell wall.^{102,108,111} Subsequent unravelling and delamination of secondary cell wall was credited to the dissolution of hemicellulose as well as defibrillation of cellulose. Biomass regenerated after complete IL-dissolution displayed no semblance to the original vascular structure, indicating a loss of cellulose crystallinity as well as depolymerization of hemicellulose and lignin.^{39,40,110} Based on SEM screening, ILs with high hydrogen bond basicity were found to be ideal for swelling and disrupting the secondary and middle lamellar layers of plant cell wall, because of their favorable interactions with structural polysaccharides.¹⁰² On the other hand, ILs with low hydrogen bond basicity were favorable for interactions with lignin and subsequent delignification.¹⁰²

Nano-scale evaluation of lignocellulosic biomass using atomic force microscopy (AFM), at 100 nm to 4 μm length scales, is useful to understand the surface-level changes in

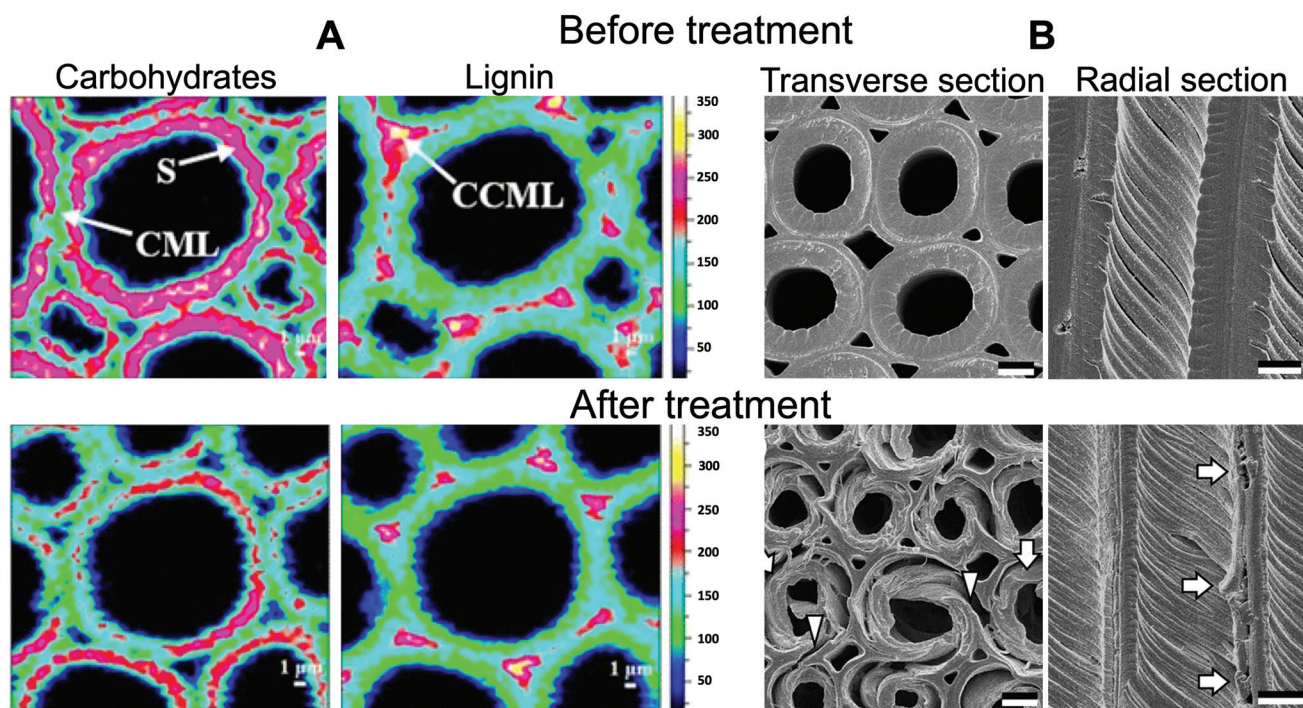


Fig. 6 (A) Changes in Eucalyptus secondary cell wall (S), compound middle lamella (CML) and cell corner middle lamella (CCML) when treated with 1-allyl-3-methylimidazolium chloride at 120 $^{\circ}\text{C}$ for 30 min. Distribution of structural polysaccharides and lignin was obtained by integrating the Raman spectra at 2830 to 2920 cm^{-1} and 1560 to 1625 cm^{-1} , respectively (adapted from ref. 108); (B) SEM images of Japanese cedar cell wall treated with 1-ethyl-3-methylimidazolium chloride at 120 $^{\circ}\text{C}$ for 72 h; scale bars are 5 μm (adapted from ref. 102).

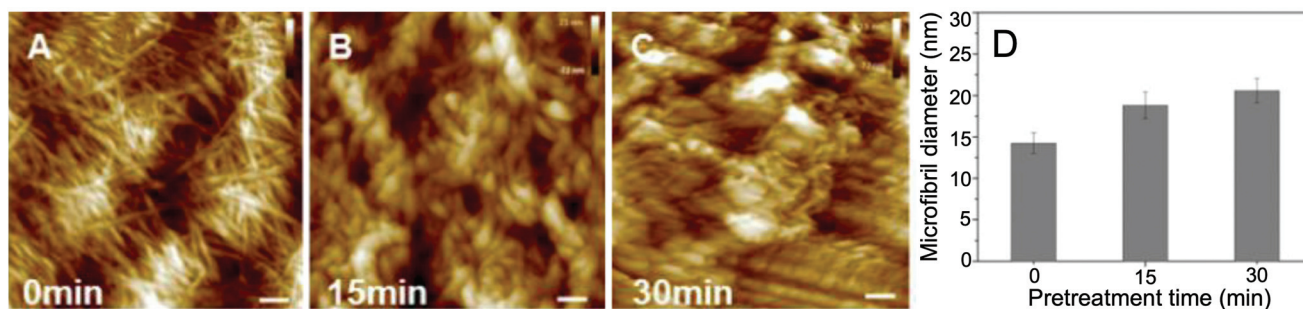


Fig. 7 (A–C) Time-dependent changes in the microfibril structure of rice straw treated with 1-ethyl-3-methylimidazolium acetate at 90 °C, determined using AFM (scale bars are 100 nm). Initially the surface roughness increased due to disruption of cellulose microfibrils but later decreased as the matrix polysaccharides were dissolved. (D) Changes in microfibril diameter calculated from AFM images as a function of treatment time. Swelling of cellulose microfibrils was observed in the presence of IL. Adapted with permission from ref. 114; copyright (2018) American Chemical Society.

structure and composition. AFM mapping of untreated plant fibers usually exhibited a smooth surface characteristic of cellulose microfibrils, along with roughness introduced by the matrix polymers of lignin and hemicellulose (Fig. 7).^{108,112} This is useful for comparisons with regenerated lignocellulosic films, which exhibited variations in surface roughness depending on lignin and hemicellulose content as well as phase separation depending on the deposition of these components.⁵⁹ AFM studies of IL-processed biomass have also shown that there is appearance of fissures as a result of disruption in microfibril bundles, followed by decrease in surface roughness as a result of removal of hemicellulose and lignin over time (Fig. 7A–C).^{108,113} In particular, AFM was used to delineate the mechanism of holocellulose dissolution in ILs, where it was determined that the initial swelling of microfibril bundles (Fig. 7D) was critical for subsequent loss of crystallinity and delamination of cellulose.¹¹⁴ Moreover, appropriate hydrogen bonding capacity as well as IL-anion and cation sizes were determined to be essential for inducing optimal swelling of holocellulose bundles.¹¹⁴

Considering all the evidences collected through microscopy and imaging studies, we can conclude that there is (1) swelling of the secondary cell wall layer as a result of hydrogen bond interactions between structural polysaccharides and ILs; (2) cracking and disruption of fiber bundles accelerates the imbibition of ILs; (3) cellulose crystallinity is reduced, and (4) the polymeric matrix *i.e.*, lignin and hemicellulose, dissolves resulting in unravelling of cell wall layers. Depolymerization of lignin, cellulose and hemicellulose may occur concurrently, however further investigation is necessary to unravel the specific chemical and physical changes.

4.2. Factors affecting cellulose crystallinity and lignocellulose ultrastructure

Since the swelling of cellulose and loss of its crystallinity are the first stages of reducing biomass recalcitrance,^{106,114} understanding the ultrastructure of cellulose *via* X-ray diffraction technique (XRD) is critical for improving IL-based processing. After regeneration from IL-treatment, cellulose often loses its orderly structure or undergo changes in planar arrangement,

which reduces its recalcitrant nature.^{115,116} Zhang *et al.* (2014) had proposed that, during IL-treatment under milder conditions (<90 °C), the cellulose crystals swelled as a result of interactions with ILs leading to reduction in $2\theta = 1\bar{1}0$ peak area at 15.6° and loss of crystallinity (Fig. 8a).¹¹⁷ Whereas, upon severe IL-treatments (>110 °C or longer durations), there was delamination of cellulose polymer chains and subsequent dissolution in ILs, which altered the cellulose polymorph, from type I to II, after regeneration (Fig. 8a and b).^{115,117} This phenomenon is detected by a shift in the $2\theta = 1\bar{1}0$ peak from 15.6° to ~12.5°.^{118,119} Several XRD experiments have shown that, *via* optimization of IL-treatment temperature, time, and solid loading, it is possible to (1) maximize swelling with minimal dissolution of cellulose and (2) convert cellulose to a lower order transitional state where there is significant reduction of crystallinity, but with a higher mass recovery.^{117,119}

In recent years, the ultrastructure of whole lignocellulosic biomass has been delineated using an advanced, small-angle neutron scattering (SANS) technique. SANS utilizes the differences in neutron scattering length density between cellulose ($1.78 \times 10^{-6} \text{ \AA}^{-2}$), hemicellulose ($1.52 \times 10^{-6} \text{ \AA}^{-2}$) and lignin ($2.21 \times 10^{-6} \text{ \AA}^{-2}$) to determine their structural differences.^{120,121} Ionic liquids have comparatively different neutron scattering length density, *e.g.* $1.14 \times 10^{-6} \text{ \AA}^{-2}$ or $6.07 \times 10^{-6} \text{ \AA}^{-2}$ for non-deuterated and deuterated 1-ethyl-3-methylimidazolium acetate, respectively,¹²² and therefore can be utilized to investigate the *in situ* changes in lignocellulose during the dissolution process. It was reported that, during switchgrass dissolution in ILs, the cellulose fibrils disassociated into individual polymer chains whereas the residual lignin and hemicellulose moieties remained intact thereby conserving the supramolecular structure (Fig. 9).¹²⁰ This network structure, formed by covalent linkages between hemicellulose and lignin (otherwise known as lignin-carbohydrate complexes), was proposed to be responsible for the swelling behavior of plant cell wall during IL-treatments.¹²⁰ *In situ* studies of individual polymers have shown that cellulose exhibited a worm-like linear structure with very high aspect ratio that was consistent with disassociation of microfibrils and molecular level interactions

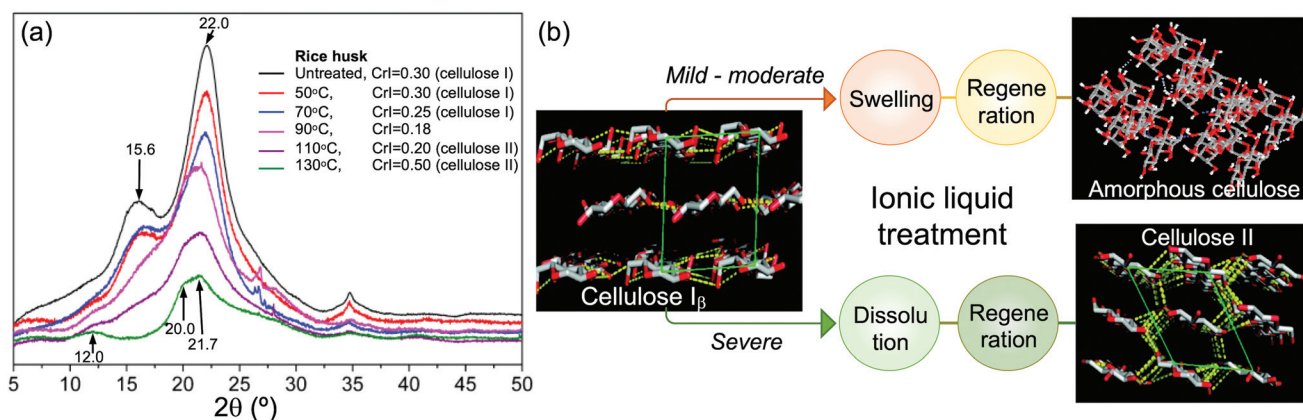


Fig. 8 (a) XRD diffractograms of rice husk pretreated with 1-butyl-3-methylimidazolium acetate at 50, 70, 90, 110, and 130 °C for 6 h. XRD peak shifts illustrate the loss of crystallinity and changes in cellulose polymorph structure from type I to II, as the treatment severity increases. Adapted from ref. 117 with permission from Elsevier. (b) Schematic illustration of mechanisms underlying the changes in cellulose crystalline structure during IL-treatment. Adapted with permission from ref. 115; copyright (2011) American Chemical Society.

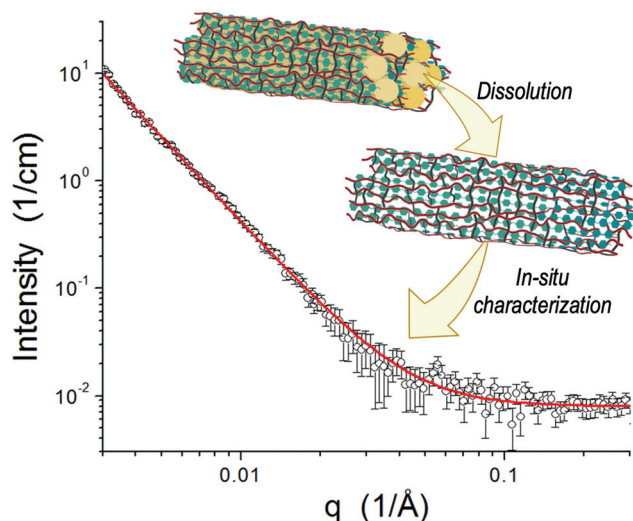


Fig. 9 Small-angle neutron scattering profile of switchgrass (open circles) fitted with a power law function (red line). Switchgrass was dissolved in 1-ethyl-3-methylimidazolium acetate at 110 °C for 44 h. The graphic illustrates how the branched structure indicated by a power law exponent of 2.64 ± 0.02 could have formed from the residual lignin and hemicellulose networks after the delamination and dissolution of cellulose microfibrils in IL. Adapted with permission from ref. 120; copyright (2014) American Chemical Society.

with ILs.¹²² However, the crystalline core of native cellulose was proposed to stay intact since there was no significant changes in the radius of gyration (R_g) even after 24 h of incubation with ILs.^{123,124} The structure of IL-treated technical lignins, like organosolv, kraft, alkali and lignosulfonate, was determined after dissolution in deuterated DMSO, and was shown to depolymerize from large aggregates (200 ± 30 nm) into nanoscale subunits ($\sim 19.7 \pm 2.1$ Å) with a defined cylindrical or ellipsoidal shape.¹²⁵ This observation was consistent with the reduction of molecular weight and loss of β -O-4 linkages as determined using gel permeation chromatography

(GPC), FTIR and NMR analyses. SANS study results have also elucidated the *in situ* changes in surface roughness of whole lignocellulose during IL-treatments; there is an initial increase in roughness as a result of disruption and delamination of cellulose microfibrils followed by smoothing out when the underlying cellulose embedded in lignin-hemicellulose matrix is exposed.¹¹⁵ The biomass surface also became smoother, during prolonged IL-treatment as a result of increase in conversion of native cellulose structure to type-II or amorphous forms.¹¹⁵ Similarly, SANS studies have shown that IL-treatment and preferential dissolution of cellulose, hemicellulose or lignin leads to increase in porosity of lignocellulosic biomass.¹²⁶

4.3. Chemical changes favoring lignocellulose dissolution in ILs

Different mechanisms are involved in the deconstruction of cellulose, hemicellulose and lignin within the plant cell wall structure. 1D proton (^1H), carbon (^{13}C) and phosphorus (^{31}P) nuclear magnetic resonance (NMR) spectroscopies, as well as 2D (^1H - ^{13}C) heteronuclear single quantum coherence (HSQC) NMR, have been previously utilized to analyze IL-biomass interactions, cellulose crystallinity, hydroxyl and other functional groups of lignocellulose, as well as lignin-carbohydrate inter-unit linkages.¹²⁷⁻¹²⁹ *In situ* ^1H and ^{13}C NMR spectroscopy of native and purified cellulose have clearly shown the formation of hydrogen bonding between its anomeric and secondary hydroxyl groups with that of the H_2 proton of IL-cations and anions.¹³⁰ To achieve a complete dissolution of cellulose, the IL-anion must exhibit good hydrogen bond accepting capacity, whereas the IL-cation could exhibit moderate hydrogen bond donating capacity but with a higher degree of dissociation.¹³⁰ Analysis of regenerated biomass has shown that ILs with highly basic anions ($\beta \geq 1.0$) caused base-catalyzed reactions between the IL-cations and C_1 , C_2 , C_6 positions of cellulose (Fig. 10). These ILs also disrupted the crystalline structure, as indicated by the reduction in corresponding peak

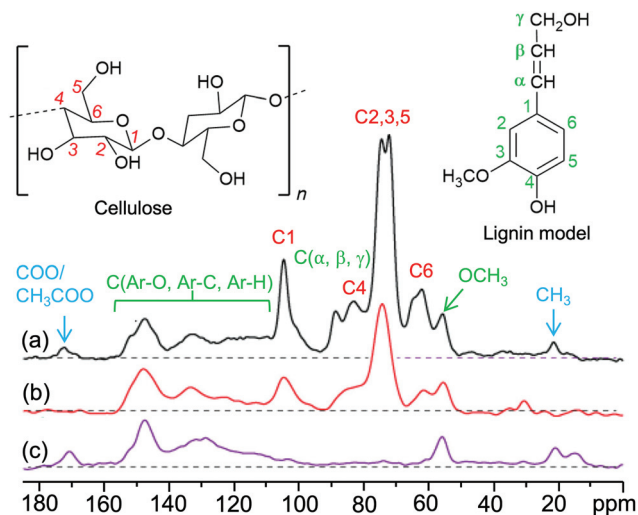


Fig. 10 Solid-state ^{13}C NMR spectra of (a) untreated, (b) 1-ethyl-3-methylimidazolium acetate and (c) 1-ethylimidazolium acetate pretreated pine powder. The red, green, and blue labels indicate contributions from cellulose, lignin, and hemicellulose fractions, respectively. Adapted with permission from ref. 131; copyright (2019) American Chemical Society.

at C_4 position (Fig. 10b and c), resulting in increased amorphous regions and accessibility of cellulose for further deconstruction.¹³¹ On the other hand, ILs containing comparatively less basic anions, like BF_4^- ($\beta < 0.6$),¹³² caused extensive swelling of cellulose fibers without significantly affecting its crystallinity. In such cases, the protic nature of ILs was believed to be responsible for preventing extensive depolymerization of crystalline cellulose, since they interact *via* reversible proton transfer mechanism unlike aprotic solvents that irreversibly disrupt the native covalent linkages.⁸⁷ Other *in situ* self-diffusion NMR studies have shown that cellulose may dissolve in aqueous ILs *via* electrostatic interactions between the hydroxyl groups.¹³³ Therefore, future *in situ* NMR studies using acetate or protic ILs may elucidate the mechanisms underlying the swelling and consequent ultrastructural changes in cellulose.

In the case of hemicellulose, three major mechanisms were determined to occur based on 2D-HSQC NMR signals corresponding to *O*-acetylated xylan, glycosidic linkages and $\text{C}_4\text{-H}_4$ correlations of 4-*O*-methyl- α -D-glucuronic acid; (1) deacetylation, (2) reduction in degree of polymerization and (3) cleavage of uronic acid side-chains.¹³⁴ The deacetylation efficiency increased with the degree of basicity of IL-anions.¹³⁴ Therefore, ILs containing highly basic anions are often used to target the hemicellulose polysaccharides during pretreatment processes and to reduce the recalcitrance of lignocellulosic biomass.

True to its complex structure, lignin undergoes depolymerization following diverse pathways depending on the nature of ILs. Common chemical changes reported to occur in lignin, based on 2D-HSQC NMR reports, are (1) up to 50% reduction of methoxy groups resulting from transformation of aromatic rings into quinonoid structures,¹³⁵ (2) almost 80% hydrolysis

of native ether (β -O-4) linkages in an acidic environment, followed by reduction and re-substitution of β - β and β -5 linkages,¹³⁶ (3) dehydration in alkaline environment and reduction of aromatic C-H species, (4) reduction of G-type lignin due to depolymerization by basic anions, or (5) reduction in S-type lignin due to demethoxylation by acidic anions,^{131,134} (6) reduction of *p*-coumaryl groups involved in lignin-carbohydrate linkages under acidic environment and corresponding increase in H-type lignin, and (7) increase in condensed 5-substituted substructures, upon prolonged exposure (>1 day) to ILs.¹³⁶ Typical *in situ* changes occurring in lignin during IL-treatment is provided in ESI Fig. S1† and the NMR chemical shifts assignments corresponding to the lignocellulosic components are provided in Table S1.†¹³⁷⁻¹⁴⁰

In situ measurement of different vibrational modes, including C-O, C=O, C-O-C, C=C, $-\text{CH}_2$, C-H, C-OH and O-H, of lignocellulosic biomass using attenuated total reflectance (ATR) - Fourier transform infrared (FTIR) spectroscopy has also been useful for high-throughput screening of ILs. Keskar *et al.* (2012) monitored the signature aromatic skeletal vibrations of lignin at 1510 cm^{-1} during dissolution in phosphonium-based ILs and calculated *in situ* quantitative losses over time.¹⁴¹ Phosphonium cations conjugated with anions having lower hydrogen bond basicity ($\beta = 0.6$) were observed to exclusively dissolve lignin from lignocellulosic biomass.^{141,142} On the other hand, when imidazolium-based ILs were implemented, a significant change was observed in the vibrational modes corresponding to conjugated C=O (1737 cm^{-1}) and C-O stretch (1233 cm^{-1}) (Fig. 11a and b).^{116,143} These changes were due to the deacetylation and dissolution of hemicellulose, which was significant for extended (>2 days) treatment durations (Fig. 11a).¹¹⁶ Furthermore, as expected, the degree of deacetylation of hemicellulose was higher for acetate ion that possessed higher pK_a and hydrogen bond basicity when compared to halides or even other carboxylate anions.^{116,143} In the case of cellulose, changes in the degree of crystallinity was determined based on the ratio of amorphous C-H bending (1375 cm^{-1}) to crystalline O-H stretching (2900 cm^{-1}). ILs with smaller cations were determined to have a greater impact on cellulose crystallinity than those having larger alkyl chain length.¹⁴⁴ It was also noted that the cellulose polymorph transformed from type I to II in the regenerated lignocellulose.¹⁴⁴ Changes in cellulose ultrastructure were induced as a result of destruction of native hydrogen bonds during interactions with ILs, and subsequent rearrangement during precipitation with an anti-solvent.¹⁴⁵ This observation was consistent with XRD measurements as indicated in a previous section (Fig. 8).

4.4. Scope for screening ILs based on lignocellulose composition and molecular weight

Quantitative information about chemical compositional changes in lignocellulosic biomass is essential for a comprehensive evaluation of IL-based processing. In addition to correlating with morphological and physical changes, measurement of chemical composition can verify the mechanistic pathways

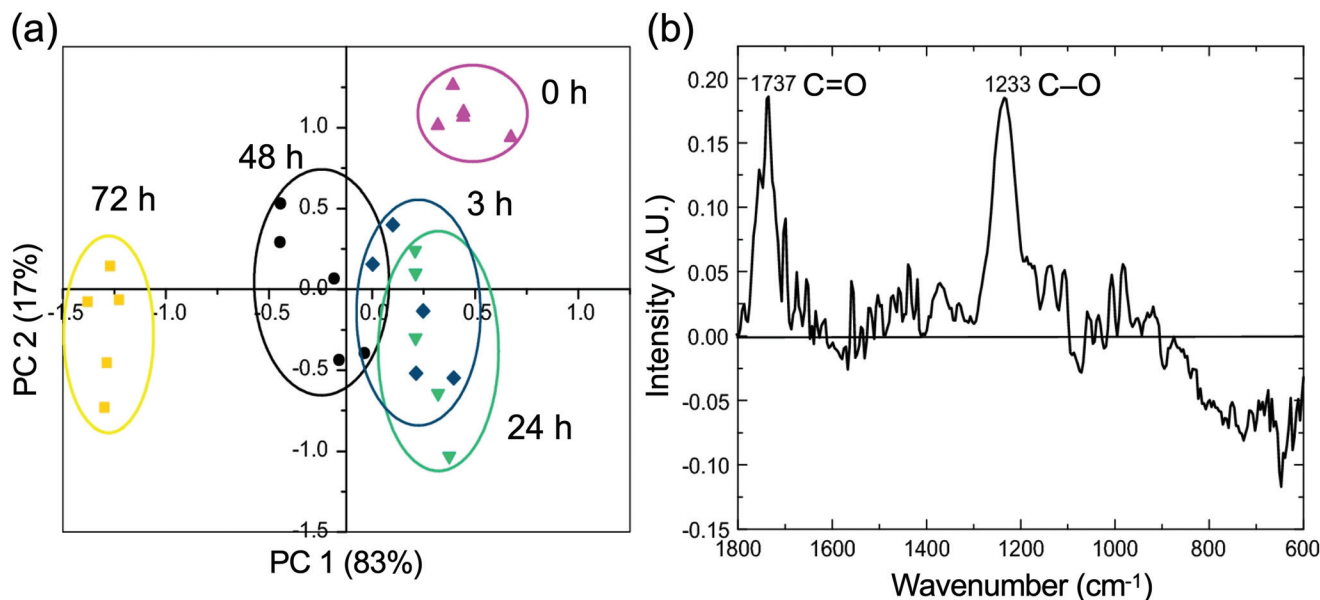


Fig. 11 (a) Principal component analysis of ATR-FTIR spectra of hybrid poplar pretreated with 1-ethyl-3-methylimidazolium acetate for different periods of time. (b) Principal component 1 (PC 1) of FTIR spectra indicated that 83% of the variances in the 72 h pretreated sample arose from fewer C=O vibrations and C–O stretch corresponding to the loss of acetyl groups of hemicellulose (adapted from ref. 116).

involved in IL-based conversion of lignocellulosic biomass. As given in Table 2, increase or decrease in lignocellulosic components provides insights about the relationship between IL composition and the relative dissolution behavior. For example, an increase in the basicity of anions in imidazolium-based ILs led to enhanced loss of acetyl and hemicellulose content.¹¹⁶ In the case of tertiary amine-based ILs, less polar cations synthesized from aromatic aldehydes were more efficient in the dissolution of lignin than the polar counterparts (Table 2).¹⁴⁶ Other than IL structure, factors like treat-

ment temperature, duration (Table 2), biomass loading and particle size will also affect the outcome. Hence, compilation of chemical composition provides the opportunity for application-based screening of ILs and for optimizing biomass recovery.

During reactions with ILs, as indicated by NMR and FTIR results, the lignocellulosic components undergo depolymerization and therefore, should exhibit changes in molecular size. A recent study measured *in situ* changes in molecular weight of cellulose by utilizing a GPC system equipped with a hydro-

Table 2 Chemical compositional changes induced by ionic liquid pretreatment of various lignocellulosic feedstocks

Ionic liquid	Biomass	Treatment conditions	Chemical compositional changes (% dry wt) ^a			Ref.
			Cellulose	Hemicellulose	Lignin	
1-Ethyl-3-methyl imidazolium acetate	Hybrid poplar	60 °C, 72 h	-1.6	-3.4	0.0	116
	Switchgrass	160 °C, 3 h	-7.7	+28.6	-52.5	146
	Energy cane	120 °C, 0.5 h	-8.8	-12.1	-32.1	147
	Wheat straw	140 °C, 2 h	-4.8	-35.2	+2.4	148
	Eucalyptus	140 °C, 2 h	-9.5	-43.3	-7.6	
1-Ethyl-3-methyl imidazolium hydrogen sulfate	Wheat straw	140 °C, 1.5 h	-9.0	-59.6	+10.7	148
	Eucalyptus	140 °C, 1.5 h	+11.8	-46.7	-3.1	
1-Allyl-3-methyl imidazolium formate	Hybrid poplar	60 °C, 72 h	-3.6	-10.2	-1.1	116
Tetrabutylammonium hydroxide	Switchgrass	50 °C, 3 h	-6.5	-69.8	-75.7	149
		160 °C, 3 h	-5.0	+23.7	-20.0	146
		160 °C, 3 h	-5.9	-14.1	-3.9	
[<i>p</i> -AnisEt ₂ NH][H ₂ PO ₄]	Switchgrass	160 °C, 3 h	-10.9	+30.4	-43.0	
Choline acetate	Corn cob	150 °C, 20 h	-6.2	-9.3	-36.0	150

^a(+) increase or (-) decrease in chemical content with respect to untreated biomass.

philic separation media, columns with large exclusion limit (100 000 kDa) and a differential refractive index/multiple angle laser scattering (dRI/MALLS) detector.¹⁵¹ The study results indicated a 37 to 43% reduction in molecular weight of commercial microcrystalline cellulose pretreated with 1-ethyl-3-methylimidazolium acetate. Moreover, there was decrease in polydispersity with the increase in hydrolysis duration which indicated a consistent depolymerization of higher molecular weight polymer chains, before subsequent degradation of small molecular weight chains. Thus, the GPC study elucidated how the molecular weight distribution of cellulose was affected by IL treatment severity. In future, similar IL-based GPC systems may be successfully adapted for *in situ* monitoring of not just cellulose but the whole lignocellulosic biomass.

During the dissolution process, viscosity of the IL-biomass mixture is affected by, among other factors, the molecular size of lignocellulose. A general rule of thumb is that, the shear viscosity of a polymer solution will increase as a function of molecular weight.¹⁵³ The Mark–Houwink equation defines this relationship as follows; $[\eta] = KM_r^\alpha$, where $[\eta]$ is the intrinsic viscosity, M_r is the relative molecular mass average, K is an empirical constant, and α is a scalar which defines the flexibility of a polymer.^{152,153} The α constant for cellulose-IL solutions ranges between 0.65–0.95 and it depends on the solute concentration, temperature and solvent type (Fig. 12).¹⁵² Commercial microcrystalline cellulose is known to exhibit a flexible state, with a scalar factor of 0.85, when dissolved in a 1 : 1 (w/w) mixture of 1-butyl-3-methylimidazolium acetate and DMSO.¹⁵⁴ Therefore, when a Mark–Houwink relationship is established between the intrinsic viscosity and molecular

weight (M_w) of cellulose dissolved in this solvent system, it provides a simple and swift method for *in situ* monitoring of molar mass.¹⁵⁴ In the beginning, intrinsic viscosity– M_w relationship is calibrated using a GPC, whereas the subsequent high-throughput characterizations are carried out using a rheometer. A similar relationship has been established for cellulose solution made with 1 : 4 (v/v) tetrabutylammonium hydroxide and DMSO.¹⁵⁵ In the future, this simple strategy can be further expanded to include whole lignocellulosic biomass as well as other IL-based solvent systems. Thus, combined with the previously described GPC method, the rheological means for estimating molecular weight provides a powerful tool for *in situ*, high-throughput quantification of changes imparted by ILs.

5. Conclusions and future perspective

To summarize, various *in situ* investigations have comprehensively described the morphological changes in plant cell wall as a result of interactions with ILs. There is consensus about typical changes observed during IL-treatments, such as bulk swelling, loss of cellulose crystallinity, unbundling and unraveling of cell wall layers and ultimate loss of structural integrity (Fig. 13). *In situ* investigations using NMR spectroscopy have elucidated the underlying chemical changes in lignin and hemicellulose that were responsible for their subsequent dissociation from the fiber bundles and depolymerization. Complementary XRD and AFM analyses have clearly shown how the upturn in cellulose fibril thickness, as a result of hydrogen bonding with ILs, induced increase in interplanar distances and led to subsequent delamination and depolymerization of cellulose microfibrils. These changes were responsible for the cracking and weakening of secondary and middle lamellar cell wall layers that enhanced IL penetration. However, changes in the ultrastructure of lignocellulose remain unclear in the subsequent stages. Although NMR studies have shown disruption in LCC (lignin-carbohydrate complexes), SANS studies provided contradictory evidence of intact network structure as a result of conservation of LCC linkages. Moreover, while AFM and SANS experiments recorded consistent changes in surface roughness during prolonged IL-treatments, whether these changes were caused by the dissolution of matrix polymers or of cellulose microfibrils is yet to be determined. These observations are further complicated by the fact that the response of lignocellulosic biomass will depend on the chemical composition and properties of the selected ILs, such as hydrogen bonding capacity, polarity, size of cations, and atom transfer mechanisms. Ancillary chemical quantification methods have clearly shown that, with some exceptions, all three lignocellulosic components are depolymerized and degraded during IL-based processing, albeit at different levels. Therefore, in order to clearly understand the physico-chemical changes undergone by lignocellulose

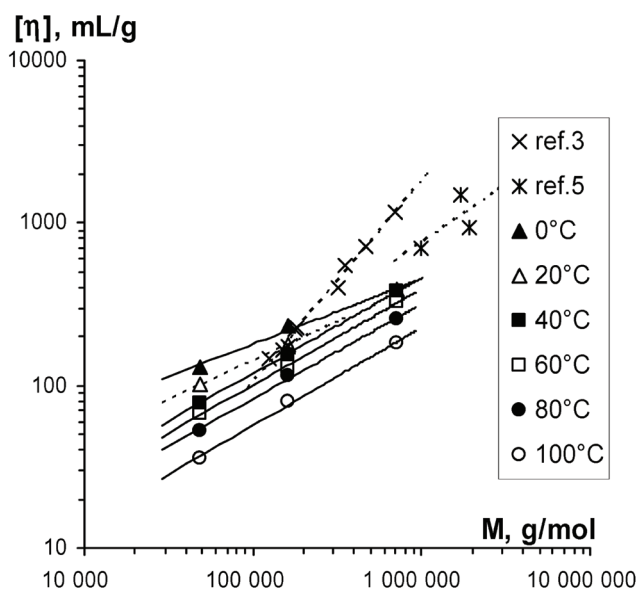


Fig. 12 Relationship between intrinsic viscosity and molecular weight of microcrystalline cellulose dissolved in 1-ethyl-3-methylimidazolium acetate, at different temperatures. Solid lines are Mark–Houwink approximations and dotted lines are for reference cellulose samples dissolved in LiCl/DMAC at 30 °C. Reprinted with permission from ref. 152; copyright (2009) American Chemical Society.

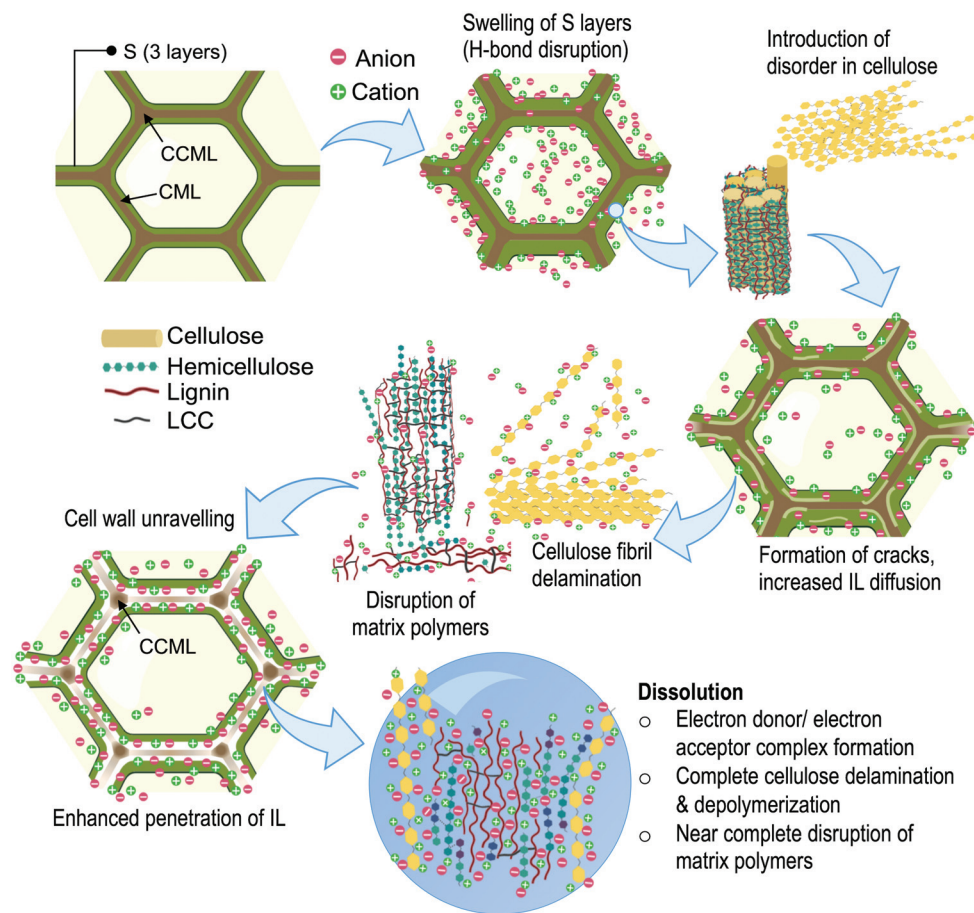


Fig. 13 Summation of morphological and physico-chemical changes underwent by lignocellulosic biomass during IL-based processing (S – secondary cell wall, CML – compound middle lamella, CCML – cell corner middle lamella, LCC – lignin carbohydrate complexes).

during the latter stages of IL-treatments, *in situ* characterizations have to be streamlined. The different characterization studies described in this review have to be constructively combined to obtain nano- and molecular-scale illustration of lignocellulosic components during IL-based processing. The streamlining strategy will be met with challenges, such as, lack of proper contrast between ILs and lignocellulose during particle scattering experiments, or of lowered resolution during *in situ* NMR and FTIR spectroscopies, which can occur as a result of strong intermolecular interactions between ILs and lignocellulose. Lack of information about critical physico-chemical properties, such as *in situ* molecular weight changes, is another hurdle. However, considering the wealth of information amassed using existing characterization experiments, combined with the broadening horizons of IL-based processing technologies, there are increasing incentives for expounding on the *in situ* state of lignocellulosic biomass.

Conflicts of interest

There are no conflicts to declare.

Acknowledgements

This research was supported by funding from the U. S. Forest Service (Award #19-JV-1130131-026) and the Southeastern Regional Sun Grant Program at the University of Tennessee through a grant provided by the U. S. Department of Agriculture (Award #2014-38502-22598).

References

- 1 P. Reddy, *S. Afr. J. Sci.*, 2015, **111**, 1–9.
- 2 J. Chen, F. Xie, X. Li and L. Chen, *Green Chem.*, 2018, **20**, 4169–4200.
- 3 M. Watanabe, M. L. Thomas, S. Zhang, K. Ueno, T. Yasuda and K. Dokko, *Chem. Rev.*, 2017, **117**, 7190–7239.
- 4 A. Stojanovic and B. K. Keppler, *Sep. Sci. Technol.*, 2012, **47**, 189–203.
- 5 J. Wang, J. Luo, S. Feng, H. Li, Y. Wan and X. Zhang, *Green Energy Environ.*, 2016, **1**, 43–61.
- 6 Y. Zhou and J. Qu, *ACS Appl. Mater. Interfaces*, 2017, **9**, 3209–3222.

- 7 H. Mahmood, M. Moniruzzaman, S. Yusup and H. M. Akil, in *Progress and developments in ionic liquids*, ed. S. Handy, IntechOpen, London, UK, 2017, ch. 6, pp. 117–131.
- 8 A. M. da Costa Lopes, K. G. João, A. R. C. Morais, E. Bogel-Lukasik and R. Bogel-Lukasik, *Sustainable Chem. Processes.*, 2013, **1**, 1–31.
- 9 M. A. Ab Rani, A. Brant, L. Crowhurst, A. Dolan, M. Lui, N. H. Hassan, J. P. Hallett, P. A. Hunt, H. Niedermeyer, J. M. Perez-Arlandis, M. Schrems, T. Welton and R. Wilding, *Phys. Chem. Chem. Phys.*, 2011, **13**, 16831–16840.
- 10 A. Brandt, J. Gräsvik, J. P. Hallett and T. Welton, *Green Chem.*, 2013, **15**, 550–583.
- 11 F. J. V. Gschwend, F. Malaret, S. Shinde, A. Brandt-Talbot and J. P. Hallett, *Green Chem.*, 2018, **20**, 3486–3498.
- 12 F. J. V. Gschwend, A. Brandt-Talbot, C. L. Chambon and J. P. Hallett, in *Ionic liquids: Current state and future directions*, Oxford University Press, Oxford, UK, 2017, ch. 9, pp. 209–223.
- 13 A. M. Asim, M. Uroos, S. Naz, M. Sultan, G. Griffin, N. Muhammad and A. S. Khan, *J. Mol. Liq.*, 2019, **287**, 110943.
- 14 M. H. Langholtz, B. J. Stokes and L. M. Eaton, *2016 Billion-ton report: Advancing domestic resources for a thriving bioeconomy*, Oak Ridge National Laboratory, Oak Ridge, TN, USA, 2016, pp. 448.
- 15 Y. Fukaya, K. Hayashi, M. Wada and H. Ohno, *Green Chem.*, 2008, **10**, 44–46.
- 16 Y. Zhang, A. Xu, B. Lu, Z. Li and J. Wang, *Carbohydr. Polym.*, 2015, **117**, 666–672.
- 17 W. E. S. Hart, J. B. Harper and L. Aldous, *Green Chem.*, 2015, **17**, 214–218.
- 18 T. Akiba, A. Tsurumaki and H. Ohno, *Green Chem.*, 2017, **19**, 2260–2265.
- 19 M. Abe, K. Kuroda, D. Sato, H. Kunimura and H. Ohno, *Phys. Chem. Chem. Phys.*, 2015, **17**, 32276–32282.
- 20 A. W. King, J. Asikkala, I. Mutikainen, P. Järvi and I. Kilpeläinen, *Angew. Chem., Int. Ed. Engl.*, 2011, **50**, 6301–6305.
- 21 M. J. Kamlet and R. W. Taft, *J. Am. Chem. Soc.*, 1976, **98**, 377–383.
- 22 M. J. Kamlet, J. L. Abboud and R. W. Taft, *J. Am. Chem. Soc.*, 1977, **99**, 6027–6038.
- 23 C. G. Yoo, Y. Pu and A. J. Ragauskas, *Curr. Opin. Green Sustain. Chem.*, 2017, **5**, 5–11.
- 24 R. Ruan, Y. Zhang, P. Chen, S. Liu, L. Fan, N. Zhou, K. Ding, P. Peng, M. Addy, Y. Cheng, E. Anderson, Y. Wang, Y. Liu, H. Le and B. Li, in *Biofuels: Alternative feedstocks and conversion processes for the production of liquid and gaseous biofuels*, ed. A. Pandey, C. Larroche, C.-G. Dussap, E. Gnansounou, S. K. Khanal and S. Ricke, Academic Press, Cambridge, MA, 2nd edn, 2019, pp. 3–43.
- 25 R. Vinoth Kumar, K. Pakshirajan and G. Pugazhenthii, in *Platform chemical biorefinery*, ed. S. K. Brar, S. J. Sarma and K. Pakshirajan, Elsevier, Cambridge, MA, 1st edn, 2017, ch. 3, pp. 33–53.
- 26 A. Milbrandt and S. Booth, *Carbon fiber from biomass*, Clean Energy Manufacturing Analysis Center, Golden, CO, USA, 2016, pp. 1–10.
- 27 A. Dotan, in *Handbook of thermoset plastics*, ed. H. Dodiuk and S. H. Goodman, Elsevier, Cambridge, MA, 3rd edn, 2014, ch. 15, pp. 577–622.
- 28 W. C. Lum, S. H. Lee, Z. Ahmad, J. A. Halip and K. L. Chin, in *Industrial applications of nanomaterials*, ed. S. Thomas, Y. Grohens and Y. B. Pottathara, Elsevier, Cambridge, MA, 2019, ch. 15, pp. 423–439.
- 29 E. Fortunati, J. M. Kenny and L. Torre, in *Biomass, bio-polymer-based materials, and bioenergy*, ed. D. Verma, E. Fortunati, S. Jain and X. Zhang, Woodhead Publishing, 2019, ch. 5, pp. 87–102.
- 30 R. P. Swatloski, S. K. Spear, J. D. Holbrey and R. D. Rogers, *J. Am. Chem. Soc.*, 2002, **124**, 4974–4975.
- 31 I. Kilpeläinen, H. Xie, A. King, M. Granstrom, S. Heikkinen and D. S. Argyropoulos, *J. Agric. Food Chem.*, 2007, **55**, 9142–9148.
- 32 A. Parviainen, R. Wahlström, U. Liimatainen, T. Liitiä, S. Rovio, J. K. J. Helminen, U. Hyväkkö, A. W. T. King, A. Suurnäkki and I. Kilpeläinen, *RSC Adv.*, 2015, **5**, 69728–69737.
- 33 M. Mora-Pale, L. Meli, T. V. Doherty, R. J. Linhardt and J. S. Dordick, *Biotechnol. Bioeng.*, 2011, **108**, 1229–1245.
- 34 C. Li, B. Knierim, C. Manisseri, R. Arora, H. V. Scheller, M. Auer, K. P. Vogel, B. A. Simmons and S. Singh, *Bioresour. Technol.*, 2010, **101**, 4900–4906.
- 35 M. Mohammadi, M. Shafiei, A. Abdolmaleki, K. Karimi, J.-P. Mikkola and C. Larsson, *Ind. Crops Prod.*, 2019, **139**, 111494.
- 36 P. Nargotra, V. Sharma, M. Gupta, S. Kour and B. K. Bajaj, *Bioresour. Technol.*, 2018, **267**, 560–568.
- 37 X.-D. Hou, N. Li and M.-H. Zong, *ACS Sustainable Chem. Eng.*, 2013, **1**, 519–526.
- 38 X.-D. Hou, J. Xu, N. Li and M.-H. Zong, *Biotechnol. Bioeng.*, 2015, **112**, 65–73.
- 39 S. S. Mohtar, T. N. Z. Tengku Malim Busu, A. M. Md Noor, N. Shaari and H. Mat, *Carbohydr. Polym.*, 2017, **166**, 291–299.
- 40 M. Lara-Serrano, S. Morales-delaRosa, J. M. Campos-Martín and J. L. G. Fierro, *Appl. Sci.*, 2019, **9**, 1862.
- 41 F. Cheng, H. Wang, G. Chatel, G. Gurau and R. D. Rogers, *Bioresour. Technol.*, 2014, **164**, 394–401.
- 42 Y. Hamada, K. Yoshida, R.-I. Asai, S. Hayase, T. Nokami, S. Izumi and T. Itoh, *Green Chem.*, 2013, **15**, 1863–1868.
- 43 J. B. Binder and R. T. Raines, *J. Am. Chem. Soc.*, 2009, **131**, 1979–1985.
- 44 B. M. Matsagar, S. A. Hossain, T. Islam, H. R. Alamri, Z. A. Alothman, Y. Yamauchi, P. L. Dhepe and K. C.-W. Wu, *Sci. Rep.*, 2017, **7**, 13508.
- 45 H. Wang, Y. Zhao, Z. Ke, B. Yu, R. Li, Y. Wu, Z. Wang, J. Han and Z. Liu, *Chem. Commun.*, 2019, **55**, 3069–3072.

- 46 A. S. Khan, Z. Man, M. A. Bustam, A. Nasrullah, Z. Ullah, A. Sarwono, F. U. Shah and N. Muhammad, *Carbohydr. Polym.*, 2018, **181**, 208–214.
- 47 F. Liu, Q. Liu, A. Wang and T. Zhang, *ACS Sustainable Chem. Eng.*, 2016, **4**, 3850–3856.
- 48 P. Varanasi, P. Singh, M. Auer, P. D. Adams, B. A. Simmons and S. Singh, *Biotechnol. Biofuels*, 2013, **6**, 14.
- 49 B. J. Cox and J. G. Ekerdt, *Bioresour. Technol.*, 2012, **118**, 584–588.
- 50 K. Stärk, N. Taccardi, A. Bösmann and P. Wasserscheid, *ChemSusChem*, 2010, **3**, 719–723.
- 51 L. Das, S. Xu and J. Shi, *Front. Energy Res.*, 2017, **5**, 1–21.
- 52 K. Yamamoto, T. Hosoya, K. Yoshioka, H. Miyafuji, H. Ohno and T. Yamada, *ACS Sustainable Chem. Eng.*, 2017, **5**, 10111–10115.
- 53 B. Li, I. Filpponen and D. S. Argyropoulos, *Ind. Eng. Chem. Res.*, 2010, **49**, 3126–3136.
- 54 J. Tao, T. Kishimoto, M. Hamada and N. Nakajima, *Holzforchung*, 2017, **71**, 21–26.
- 55 B. Tisserat, E. Larson, D. Gray, N. Dexter, C. Meunier, L. Moore and L. Haverhals, *Int. J. Polym. Sci.*, 2015, **2015**, 8.
- 56 H. Mahmood, M. Moniruzzaman, T. Iqbal and S. Yusup, *J. Mol. Liq.*, 2017, **247**, 164–170.
- 57 K. Zhang, H. Xiao, Y. Su, Y. Wu, Y. Cui and M. Li, *BioResources*, 2019, **14**, 2584–2595.
- 58 A. Khosravani, M. Pourjafar and R. Behrooz, *IOP Conf. Ser.: Mater. Sci. Eng.*, 2018, **368**, 12029.
- 59 J. Wang, R. Boy, N. A. Nguyen, J. K. Keum, D. A. Cullen, J. Chen, M. Soliman, K. C. Littrell, D. Harper, L. Tetard, T. G. Rials, A. K. Naskar and N. Labbé, *ACS Sustainable Chem. Eng.*, 2017, **5**, 8044–8052.
- 60 D. H. A. T. Gunasekera, S. Kuek, D. Hasanaj, Y. He, C. Tuck, A. K. Croft and R. D. Wildman, *Faraday Discuss.*, 2016, **190**, 509–523.
- 61 K. Markstedt, J. Sundberg and P. Gatenholm, *3D Print. Addit. Manuf.*, 2014, **1**, 115–121.
- 62 N. Sun, W. Li, B. Stoner, X. Jiang, X. Lu and R. D. Rogers, *Green Chem.*, 2011, **13**, 1158–1161.
- 63 N. A. Nguyen, K. Kim, C. C. Bowland, J. K. Keum, L. T. Kearney, N. André, N. Labbé and A. K. Naskar, *Green Chem.*, 2019, **21**, 4354–4367.
- 64 Y. Ma, S. Asaadi, L. S. Johansson, P. Ahvenainen, M. Reza, M. Alekhina, L. Rautkari, A. Michud, L. Hauru, M. Hummel and H. Sixta, *ChemSusChem*, 2015, **8**, 4030–4039.
- 65 Y. Kang, Y. Ahn, S. H. Lee, J. H. Hong, M. K. Ku and H. Kim, *Fibers Polym.*, 2013, **14**, 530–536.
- 66 S. Borysiak, A. Grzabka-Zasadzińska, M. Odalanowska, A. Skrzypczak and I. Ratajczak, *Cellulose*, 2018, **25**, 4639–4652.
- 67 R. Nishita, K. Kuroda, S. Suzuki, K. Ninomiya and K. Takahashi, *Polym. J.*, 2019, **51**, 781–789.
- 68 S. Suzuki, Y. Shibata, D. Hirose, T. Endo, K. Ninomiya, R. Kakuchi and K. Takahashi, *RSC Adv.*, 2018, **8**, 21768–21776.
- 69 D. Hirose, S. B. W. Kusuma, D. Ina, N. Wada and K. Takahashi, *Green Chem.*, 2019, **21**, 4927–4931.
- 70 C. Roata, C. Croitoru, A. Pascu and E. M. Stanciu, *BioResources*, 2018, **13**, 6110–6121.
- 71 F. Xu, J. Sun, M. N. V. S. N. Konda, J. Shi, T. Dutta, C. D. Scown, B. A. Simmons and S. Singh, *Energy Environ. Sci.*, 2016, **9**, 1042–1049.
- 72 K. Ohira, Y. Abe, M. Kawatsura, K. Suzuki, M. Mizuno, Y. Amano and T. Itoh, *ChemSusChem*, 2012, **5**, 388–391.
- 73 M. Stepan, A. Michud, S. Hellstén, M. Hummel and H. Sixta, *Ind. Eng. Chem. Res.*, 2016, **55**, 8225–8233.
- 74 F. Cheng, X. Zhao and Y. Hua, *Bioresour. Technol.*, 2018, **249**, 969–975.
- 75 J. B. Binder and R. T. Raines, *J. Am. Chem. Soc.*, 2009, **131**, 1979–1985.
- 76 C. Reichardt, *Green Chem.*, 2005, **7**, 339–351.
- 77 D. J. Eyckens and L. C. Henderson, *Front. Chem.*, 2019, **7**, 263.
- 78 W. Guan, N. Chang, L. Yang, X. Bu, J. Wei and Q. Liu, *J. Chem. Eng. Data*, 2017, **62**, 2610–2616.
- 79 S. Spange, R. Lungwitz and A. Schade, *J. Mol. Liq.*, 2014, **192**, 137–143.
- 80 J. Zhang, J. Wu, J. Yu, X. Zhang, J. He and J. Zhang, *Mater. Chem. Front.*, 2017, **1**, 1273–1290.
- 81 Y. Li, J. Wang, X. Liu and S. Zhang, *Chem. Sci.*, 2018, **7**, 4027–4043.
- 82 F. M. Cláudio, L. Swift, J. P. Hallett, T. Welton, J. A. P. Coutinho and M. G. Freire, *Phys. Chem. Chem. Phys.*, 2014, **16**, 6593–6601.
- 83 V. Venkatraman and K. C. Lethesh, *Front. Chem.*, 2019, **7**, 605.
- 84 P. Moyer, M. D. Smith, N. Abdoulmoumine, S. C. Chmely, J. C. Smith, L. Petridis and N. Labbé, *Phys. Chem. Chem. Phys.*, 2018, **20**, 2508–2516.
- 85 R. S. Payal and S. Balasubramanian, *Phys. Chem. Chem. Phys.*, 2014, **16**, 17458–17465.
- 86 J. Zubeltzu, E. Formoso and E. Rezabal, *J. Mol. Liq.*, 2020, **303**, 112588.
- 87 D. L. Minnick, R. A. Flores, M. R. DeStefano and A. M. Scurto, *J. Phys. Chem. B*, 2016, **120**, 7906–7919.
- 88 G. Gogoi and S. Hazarika, *Korean J. Chem. Eng.*, 2019, **36**, 1626–1636.
- 89 R. Rinaldi, *Chem. Commun.*, 2011, **47**, 511–513.
- 90 K. Ohira, K. Yoshida, S. Hayase and T. Itoh, *Chem. Lett.*, 2012, **41**, 987–989.
- 91 Y. Dong, T. Takeshita, H. Miyafuji, T. Nokami and T. Itoh, *Bull. Chem. Soc. Jpn.*, 2018, **91**, 398–404.
- 92 Q. Zhang, X. Tan, W. Wang, Q. Yu, Q. Wang, C. Miao, Y. Guo, X. Zhuang and Z. Yuan, *ACS Sustainable Chem. Eng.*, 2019, **7**, 8678–8686.
- 93 Z. Xue, X. Zhao, R. C. Sun and T. Mu, *ACS Sustainable Chem. Eng.*, 2016, **4**, 3864–3870.
- 94 J. Spronsen, M. A. T. Cardoso, G.-J. Witkamp, W. Jong and M. C. Kroon, *Chem. Eng. Process.*, 2011, **50**, 196–199.
- 95 L. Zhao, Q. Wang and K. Ma, *ACS Sustainable Chem. Eng.*, 2019, **7**, 10544–10551.

- 96 Y. Agata and H. Yamamoto, *Chem. Phys.*, 2018, **513**, 165–173.
- 97 P. Weerachanchai, Y. Wong, K. H. Lim, T. T. Y. Tan and J.-M. Lee, *ChemPhysChem*, 2014, **15**, 3580–3591.
- 98 M. Zavrel, D. Bross, M. Funke, J. Büchs and A. C. Spiess, *Bioresour. Technol.*, 2009, **100**, 2580–2587.
- 99 M. FitzPatrick, P. Champagne, M. F. Cunningham and C. Falkenburger, *Can. J. Chem. Eng.*, 2012, **90**, 1142–1152.
- 100 H. Miyafuji and N. Suzuki, *J. Wood Sci.*, 2011, **57**, 459–461.
- 101 H. H. Myint, W. Kurniawan, H. Hinode, N. N. Sein and J. S. Cross, *ASEAN Eng. J. B*, 2016, **5**, 5–18.
- 102 T. Kanbayashi and H. Miyafuji, *Sci. Rep.*, 2016, **6**, 30147.
- 103 Y.-H. Tseng, Y.-Y. Lee and S.-H. Chen, *Appl. Sci.*, 2019, **9**, 1750.
- 104 J.-M. Andanson, E. Bordes, J. Devémy, F. Leroux, A. A. H. Pádua and M. F. C. Gomes, *Green Chem.*, 2014, **16**, 2528–2538.
- 105 S. Singh, B. A. Simmons and K. P. Vogel, *Biotechnol. Bioeng.*, 2009, **104**, 68–75.
- 106 X. Zhang, J. Ma, Z. Ji, G. H. Yang, X. Zhou and F. Xu, *Microsc. Res. Tech.*, 2014, **77**, 609–618.
- 107 L. Sun, C. Li, Z. Xue, B. A. Simmons and S. Singh, *RSC Adv.*, 2013, **3**, 2017–2027.
- 108 H.-Y. Li, X. Chen, C.-Z. Wang, S.-N. Sun and R.-C. Sun, *Biotechnol. Biofuels*, 2016, **9**, 166.
- 109 H. Coceancigh, D. A. Higgins and T. Ito, *Anal. Chem.*, 2019, **91**, 405–424.
- 110 T. N. Ang, G. C. Ngoh, A. S. M. Chua and M. G. Lee, *Biotechnol. Biofuels*, 2012, **5**, 67.
- 111 K. M. Torr, K. T. Love, Ö. P. Çetinkol, L. A. Donaldson, A. George, B. M. Holmes and B. A. Simmons, *Green Chem.*, 2012, **14**, 778–787.
- 112 A. M. Charrier, A. L. Lereu, A. L. Farahi, B. H. Davison and B. H. Passian, *Front. Energy Res.*, 2018, **6**, 11.
- 113 I. Kaur and G. Sahni, *Green Sustainable Chem.*, 2018, **8**, 92–114.
- 114 J. Xu, B. Zhang, X. Lu, Y. Zhou, J. Fang, Y. Li and S. Zhang, *ACS Sustainable Chem. Eng.*, 2018, **6**, 909–917.
- 115 G. Cheng, P. Varanasi, C. Li, H. Liu, Y. B. Melnichenko, B. A. Simmons, M. S. Kent and S. Singh, *Biomacromolecules*, 2011, **12**, 933–941.
- 116 P. Moyer, K. Kim, N. Abdoulmoumine, S. C. Chmely, B. K. Long, D. J. Carrier and N. Labbé, *Biotechnol. Biofuels*, 2018, **11**, 265.
- 117 J. Zhang, Y. Wang, L. Zhang, R. Zhang, G. Liu and G. Cheng, *Bioresour. Technol.*, 2014, **151**, 402–405.
- 118 A. D. French, *Cellulose*, 2014, **21**, 885–896.
- 119 Z. Ling, S. Chen, X. Zhang, K. Takabe and F. Xu, *Sci. Rep.*, 2017, **7**, 10230.
- 120 H. Wang, G. Gurau, S. V. Pingali, H. M. O'Neill, B. R. Evans, V. S. Urban, W. T. Heller and R. D. Rogers, *ACS Sustainable Chem. Eng.*, 2014, **2**, 1264–1269.
- 121 G. Cheng, X. Zhang, B. Simmons and S. Singh, *Energy Environ. Sci.*, 2015, **8**, 436–455.
- 122 V. S. Raghuwanshi, Y. Cohen, G. Garnier, C. J. Garvey, R. A. Russell, T. Darwish and G. Garnier, *Macromolecules*, 2018, **51**, 7649–7655.
- 123 S. P. S. Chundawat, L. D. C. Sousa, S. Roy, Z. Yang, S. Gupta, R. Pal, C. Zhao, S.-H. Liu, L. Petridis, H. O'Neill and S. V. Pingali, *Green Chem.*, 2020, **22**, 204–218.
- 124 J. Viell, H. Inouye, N. K. Szekely, H. Frielinghaus, C. Marks, Y. Wang, N. Anders, A. C. Spiess and L. Makowski, *Biotechnol. Biofuels*, 2016, **9**, 7.
- 125 G. Cheng, M. S. Kent, L. He, P. Varanasi, D. Dibble, R. Arora, K. Deng, K. Hong, Y. B. Melnichenko, B. A. Simmons and S. Singh, *Langmuir*, 2012, **28**, 11850–11857.
- 126 X. Yuan, Y. Duan, L. He, S. Singh, B. Simmons and G. Cheng, *Bioresour. Technol.*, 2017, **232**, 113–118.
- 127 K. Saha, P. Dwibedi, A. Ghosh, J. Sikder, S. Chakraborty and S. Curcio, *3 Biotech*, 2018, **8**, 374.
- 128 F.-L. Wang, S. Li, Y.-X. Sun, H.-Y. Han, B.-X. Zhang, B.-Z. Hu, Y.-F. Gao and X.-M. Hu, *RSC Adv.*, 2017, **7**, 47990–47998.
- 129 H. Ben, X. Chen, G. Han, Y. Shao, W. Jiang, Y. Pu and A. J. Ragauskas, *Front. Energy Res.*, 2018, **6**, 13.
- 130 J. Zhang, H. Zhang, J. Wu, J. Zhang, J. Hea and J. Xiang, *Phys. Chem. Chem. Phys.*, 2010, **12**, 1941–1947.
- 131 M. M. Hossain, A. Rawal and L. Aldous, *ACS Sustainable Chem. Eng.*, 2019, **7**, 11928–11936.
- 132 J. M. Lopes, M. D. Bermejo, Á. Martín and M. J. Cocero, *ChemEngineering*, 2017, **1**, 1–28.
- 133 L. Gentile and U. Olsson, *Cellulose*, 2016, **23**, 2753–2758.
- 134 K. H. Kim, T. Dutta, J. Ralph, S. D. Mansfield, B. A. Simmons and S. Singh, *Biotechnol. Biofuels*, 2017, **10**, 101.
- 135 Y. Qu, H. Luo, H. Li and J. Xu, *Biotechnol. Rep.*, 2015, **6**, 1–7.
- 136 A. Brandt-Talbot, F. J. V. Gschwend, P. S. Fennell, T. M. Lammens, B. Tan, J. Weale and J. P. Hallett, *Green Chem.*, 2017, **19**, 3078–3102.
- 137 K. M. Holtman, N. Chen, M. A. Chappell, J. F. Kadla, L. Xu and J. Mao, *J. Agric. Food Chem.*, 2010, **58**, 9882–9892.
- 138 J.-L. Wen, Y.-C. Sun, F. Xu and R.-C. Sun, *J. Agric. Food Chem.*, 2010, **58**, 11372–11383.
- 139 Y. Pu, S. Cao and A. J. Ragauskas, *Energy Environ. Sci.*, 2011, **4**, 3154–3166.
- 140 M. Balakshin and E. Capanema, *J. Wood Chem. Technol.*, 2015, **35**, 220–237.
- 141 S. S. Keskar, L. A. Edye, C. M. Fellows and W. O. S. Doherty, *J. Wood Chem. Technol.*, 2012, **32**, 175–186.
- 142 A. J. Holding, M. Heikkilä, I. Kilpeläinen and A. W. T. King, *ChemSusChem*, 2014, **7**, 1422–1434.
- 143 N. Labbé, L. M. Kline, L. Moens, K. Kim, P. C. Kim and D. G. Hayes, *Bioresour. Technol.*, 2012, **104**, 701–707.
- 144 N. Muhammad, Z. Man, M. I. A. Mutalib, M. A. Bustam, C. D. Wilfred, A. S. Khan, Z. Ullah, G. Gonfa and A. Nasrullah, *ChemBioEng Rev.*, 2015, **2**, 257–278.
- 145 X. Zhang, N. Xiao, H. Wang, C. Liu and X. Pan, *Polymers*, 2018, **10**, 614.

- 146 A. M. Socha, R. Parthasarathi, J. Shi, S. Pattathil, D. Whyte, M. Bergeron, A. George, K. Tran, V. Stavila, S. Venkatachalam, M. G. Hahn, B. A. Simmons and S. Singh, *Proc. Natl. Acad. Sci. U. S. A.*, 2014, **111**, E3587–E3595.
- 147 Z. Qiu and G. M. Aita, *Bioresour. Technol.*, 2013, **129**, 532–537.
- 148 J. R. Bernardo, F. M. Gírio and R. M. Lukasik, *Molecules*, 2019, **24**, 808.
- 149 R. Parthasarathi, J. Sun, T. Dutta, N. Sun, S. Pattathil, N. V. S. N. M. Konda, A. G. Peralta, B. A. Simmons and S. Singh, *Biotechnol. Biofuels*, 2016, **9**, 160.
- 150 U. Rofiqah, A. Kurniawan and R. W. Nugroho Aji, *J. Phys.: Conf. Ser.*, 2019, **1373**, 012018.
- 151 P. Engel, L. Hein and A. C. Spiess, *Biotechnol. Biofuels*, 2012, **5**, 77.
- 152 M. Gericke, K. Schlufter, T. Liebert, T. Heinze and T. Budtova, *Biomacromolecules*, 2009, **10**, 1188–1194.
- 153 W.-M. Kulicke and R. Kniewske, *Rheol. Acta*, 1984, **23**, 75–83.
- 154 J. Liu, J. Zhang, B. Zhang, X. Zhang, L. Xu, J. Zhang, J. He and C.-Y. Liu, *Cellulose*, 2016, **23**, 2341–2348.
- 155 D. Bu, X. Hu, Z. Yang, X. Yang, W. Wei, M. Jiang, Z. Zhou and A. Zaman, *Polymers*, 2019, **11**, 1605.